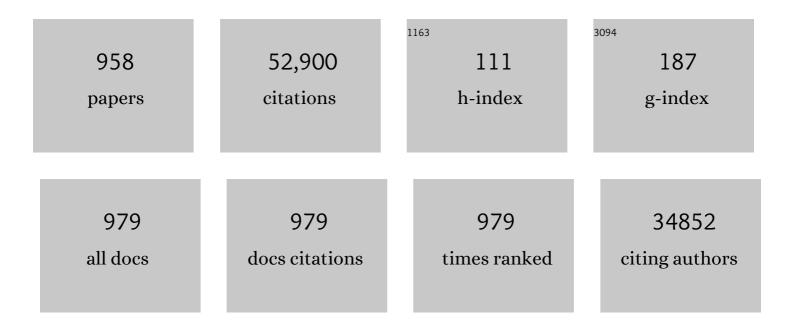
## **Dinggang Shen**

List of Publications by Year in descending order

Source: https://exaly.com/author-pdf/6192494/publications.pdf Version: 2024-02-01



DINCOMIC SHEN

#	Article	IF	CITATIONS
1	Deep Learning in Medical Image Analysis. Annual Review of Biomedical Engineering, 2017, 19, 221-248.	5.7	2,935
2	Multimodal classification of Alzheimer's disease and mild cognitive impairment. NeuroImage, 2011, 55, 856-867.	2.1	1,081
3	Detection and quantification of mutations in the plasma of patients with colorectal tumors. Proceedings of the National Academy of Sciences of the United States of America, 2005, 102, 16368-16373.	3.3	1,049
4	HAMMER: hierarchical attribute matching mechanism for elastic registration. IEEE Transactions on Medical Imaging, 2002, 21, 1421-1439.	5.4	953
5	Review of Artificial Intelligence Techniques in Imaging Data Acquisition, Segmentation, and Diagnosis for COVID-19. IEEE Reviews in Biomedical Engineering, 2021, 14, 4-15.	13.1	894
6	Hierarchical feature representation and multimodal fusion with deep learning for AD/MCI diagnosis. NeuroImage, 2014, 101, 569-582.	2.1	732
7	Deep convolutional neural networks for multi-modality isointense infant brain image segmentation. NeuroImage, 2015, 108, 214-224.	2.1	662
8	Multi-modal multi-task learning for joint prediction of multiple regression and classification variables in Alzheimer's disease. NeuroImage, 2012, 59, 895-907.	2.1	576
9	Computer-Aided Diagnosis with Deep Learning Architecture: Applications to Breast Lesions in US Images and Pulmonary Nodules in CT Scans. Scientific Reports, 2016, 6, 24454.	1.6	488
10	Evidence on the emergence of the brain's default network from 2-week-old to 2-year-old healthy pediatric subjects. Proceedings of the National Academy of Sciences of the United States of America, 2009, 106, 6790-6795.	3.3	480
11	Infant Brain Atlases from Neonates to 1- and 2-Year-Olds. PLoS ONE, 2011, 6, e18746.	1.1	458
12	Longitudinal pattern of regional brain volume change differentiates normal aging from MCI. Neurology, 2009, 72, 1906-1913.	1.5	443
13	Latent feature representation with stacked auto-encoder for AD/MCI diagnosis. Brain Structure and Function, 2015, 220, 841-859.	1.2	435
14	Medical Image Synthesis with Deep Convolutional Adversarial Networks. IEEE Transactions on Biomedical Engineering, 2018, 65, 2720-2730.	2.5	392
15	Longitudinal Development of Cortical and Subcortical Gray Matter from Birth to 2 Years. Cerebral Cortex, 2012, 22, 2478-2485.	1.6	377
16	Detection of prodromal Alzheimer's disease via pattern classification of magnetic resonance imaging. Neurobiology of Aging, 2008, 29, 514-523.	1.5	343
17	Identification of MCI individuals using structural and functional connectivity networks. NeuroImage, 2012, 59, 2045-2056.	2.1	334
18	Medical Image Synthesis with Context-Aware Generative Adversarial Networks. Lecture Notes in Computer Science, 2017, 10435, 417-425.	1.0	321

#	Article	IF	CITATIONS
19	COMPARE: Classification of Morphological Patterns Using Adaptive Regional Elements. IEEE Transactions on Medical Imaging, 2007, 26, 93-105.	5.4	320
20	Morphological classification of brains via high-dimensional shape transformations and machine learning methods. NeuroImage, 2004, 21, 46-57.	2.1	304
21	Landmark-based deep multi-instance learning for brain disease diagnosis. Medical Image Analysis, 2018, 43, 157-168.	7.0	302
22	3D conditional generative adversarial networks for high-quality PET image estimation at low dose. NeuroImage, 2018, 174, 550-562.	2.1	298
23	Hierarchical Fully Convolutional Network for Joint Atrophy Localization and Alzheimer's Disease Diagnosis Using Structural MRI. IEEE Transactions on Pattern Analysis and Machine Intelligence, 2020, 42, 880-893.	9.7	298
24	Dual-Sampling Attention Network for Diagnosis of COVID-19 From Community Acquired Pneumonia. IEEE Transactions on Medical Imaging, 2020, 39, 2595-2605.	5.4	293
25	Dynamic Development of Regional Cortical Thickness and Surface Area in Early Childhood. Cerebral Cortex, 2015, 25, 2204-2212.	1.6	286
26	Ensemble sparse classification of Alzheimer's disease. NeuroImage, 2012, 60, 1106-1116.	2.1	278
27	Deep Learning-Based Feature Representation for AD/MCI Classification. Lecture Notes in Computer Science, 2013, 16, 583-590.	1.0	269
28	A Multi-Organ Nucleus Segmentation Challenge. IEEE Transactions on Medical Imaging, 2020, 39, 1380-1391.	5.4	259
29	Deep Learning Based Imaging Data Completion for Improved Brain Disease Diagnosis. Lecture Notes in Computer Science, 2014, 17, 305-312.	1.0	249
30	Whole-Brain Morphometric Study of Schizophrenia Revealing a Spatially Complex Set of Focal Abnormalities. Archives of General Psychiatry, 2005, 62, 1218.	13.8	242
31	State-space model with deep learning for functional dynamics estimation in resting-state fMRI. NeuroImage, 2016, 129, 292-307.	2.1	242
32	The UNC/UMN Baby Connectome Project (BCP): An overview of the study design and protocol development. NeuroImage, 2019, 185, 891-905.	2.1	234
33	Large-scale screening to distinguish between COVID-19 and community-acquired pneumonia using infection size-aware classification. Physics in Medicine and Biology, 2021, 66, 065031.	1.6	233
34	Predicting Future Clinical Changes of MCI Patients Using Longitudinal and Multimodal Biomarkers. PLoS ONE, 2012, 7, e33182.	1.1	226
35	Deep ensemble learning of sparse regression models for brain disease diagnosis. Medical Image Analysis, 2017, 37, 101-113.	7.0	226
36	Temporal and Spatial Evolution of Brain Network Topology during the First Two Years of Life. PLoS ONE, 2011, 6, e25278.	1.1	224

#	Article	IF	CITATIONS
37	A Robust Deep Model for Improved Classification of AD/MCI Patients. IEEE Journal of Biomedical and Health Informatics, 2015, 19, 1610-1616.	3.9	223
38	Prediction of Alzheimer's disease and mild cognitive impairment using cortical morphological patterns. Human Brain Mapping, 2013, 34, 3411-3425.	1.9	215
39	LRTV: MR Image Super-Resolution With Low-Rank and Total Variation Regularizations. IEEE Transactions on Medical Imaging, 2015, 34, 2459-2466.	5.4	214
40	Segmentation of prostate boundaries from ultrasound images using statistical shape model. IEEE Transactions on Medical Imaging, 2003, 22, 539-551.	5.4	213
41	Scalable High-Performance Image Registration Framework by Unsupervised Deep Feature Representations Learning. IEEE Transactions on Biomedical Engineering, 2016, 63, 1505-1516.	2.5	212
42	LINKS: Learning-based multi-source IntegratioN frameworK for Segmentation of infant brain images. NeuroImage, 2015, 108, 160-172.	2.1	208
43	Estimating CT Image From MRI Data Using Structured Random Forest and Auto-Context Model. IEEE Transactions on Medical Imaging, 2016, 35, 174-183.	5.4	205
44	Deep auto-context convolutional neural networks for standard-dose PET image estimation from low-dose PET/MRI. Neurocomputing, 2017, 267, 406-416.	3.5	205
45	Highâ€order restingâ€state functional connectivity network for MCI classification. Human Brain Mapping, 2016, 37, 3282-3296.	1.9	204
46	Mapping Region-Specific Longitudinal Cortical Surface Expansion from Birth to 2 Years of Age. Cerebral Cortex, 2013, 23, 2724-2733.	1.6	203
47	Mapping Longitudinal Development of Local Cortical Gyrification in Infants from Birth to 2 Years of Age. Journal of Neuroscience, 2014, 34, 4228-4238.	1.7	203
48	BIRNet: Brain image registration using dual-supervised fully convolutional networks. Medical Image Analysis, 2019, 54, 193-206.	7.0	199
49	Brain anatomical networks in early human brain development. NeuroImage, 2011, 54, 1862-1871.	2.1	198
50	Inter-modality relationship constrained multi-modality multi-task feature selection for Alzheimer's Disease and mild cognitive impairment identification. NeuroImage, 2014, 84, 466-475.	2.1	198
51	Deformable MR Prostate Segmentation via Deep Feature Learning and Sparse Patch Matching. IEEE Transactions on Medical Imaging, 2016, 35, 1077-1089.	5.4	195
52	Joint Classification and Regression via Deep Multi-Task Multi-Channel Learning for Alzheimer's Disease Diagnosis. IEEE Transactions on Biomedical Engineering, 2019, 66, 1195-1206.	2.5	194
53	Diagnosis of Coronavirus Disease 2019 (COVID-19) With Structured Latent Multi-View Representation Learning. IEEE Transactions on Medical Imaging, 2020, 39, 2606-2614.	5.4	192
54	Enriched white matter connectivity networks for accurate identification of MCI patients. NeuroImage, 2011, 54, 1812-1822.	2.1	191

#	Article	IF	CITATIONS
55	A deep learning system for detecting diabetic retinopathy across the disease spectrum. Nature Communications, 2021, 12, 3242.	5.8	188
56	Late Fusion Incomplete Multi-View Clustering. IEEE Transactions on Pattern Analysis and Machine Intelligence, 2019, 41, 2410-2423.	9.7	187
57	Subspace Regularized Sparse Multitask Learning for Multiclass Neurodegenerative Disease Identification. IEEE Transactions on Biomedical Engineering, 2016, 63, 607-618.	2.5	181
58	Neonatal brain image segmentation in longitudinal MRI studies. NeuroImage, 2010, 49, 391-400.	2.1	177
59	A novel relational regularization feature selection method for joint regression and classification in AD diagnosis. Medical Image Analysis, 2017, 38, 205-214.	7.0	176
60	Fully convolutional networks for multi-modality isointense infant brain image segmentation. , 2016, 2016, 1342-1345.		175
61	A novel matrix-similarity based loss function for joint regression and classification in AD diagnosis. NeuroImage, 2014, 100, 91-105.	2.1	174
62	Deformable segmentation of 3-D ultrasound prostate images using statistical texture matching method. IEEE Transactions on Medical Imaging, 2006, 25, 256-272.	5.4	173
63	Effective feature learning and fusion of multimodality data using stageâ€wise deep neural network for dementia diagnosis. Human Brain Mapping, 2019, 40, 1001-1016.	1.9	171
64	Discriminant analysis of longitudinal cortical thickness changes in Alzheimer's disease using dynamic and network features. Neurobiology of Aging, 2012, 33, 427.e15-427.e30.	1.5	167
65	Development Trends of White Matter Connectivity in the First Years of Life. PLoS ONE, 2011, 6, e24678.	1.1	167
66	Relationship Induced Multi-Template Learning for Diagnosis of Alzheimer's Disease and Mild Cognitive Impairment. IEEE Transactions on Medical Imaging, 2016, 35, 1463-1474.	5.4	165
67	IDRiD: Diabetic Retinopathy – Segmentation and Grading Challenge. Medical Image Analysis, 2020, 59, 101561.	7.0	162
68	Segmentation of neonatal brain MR images using patch-driven level sets. NeuroImage, 2014, 84, 141-158.	2.1	161
69	Group-constrained sparse fMRI connectivity modeling for mild cognitive impairment identification. Brain Structure and Function, 2014, 219, 641-656.	1.2	160
70	3D Deep Learning for Multi-modal Imaging-Guided Survival Time Prediction of Brain Tumor Patients. Lecture Notes in Computer Science, 2016, 9901, 212-220.	1.0	160
71	Detecting Anatomical Landmarks for Fast Alzheimer's Disease Diagnosis. IEEE Transactions on Medical Imaging, 2016, 35, 2524-2533.	5.4	158
72	Modeling Rett Syndrome Using TALEN-Edited MECP2 Mutant Cynomolgus Monkeys. Cell, 2017, 169, 945-955.e10.	13.5	158

#	Article	IF	CITATIONS
73	An adaptive-focus statistical shape model for segmentation and shape modeling of 3-D brain structures. IEEE Transactions on Medical Imaging, 2001, 20, 257-270.	5.4	157
74	Past adult lead exposure is linked to neurodegeneration measured by brain MRI. Neurology, 2006, 66, 1476-1484.	1.5	157
75	FGFR2 amplification has prognostic significance in gastric cancer: results from a large international multicentre study. British Journal of Cancer, 2014, 110, 967-975.	2.9	154
76	Abnormal lung quantification in chest CT images of COVIDâ€19 patients with deep learning and its application to severity prediction. Medical Physics, 2021, 48, 1633-1645.	1.6	154
77	DICCCOL: Dense Individualized and Common Connectivity-Based Cortical Landmarks. Cerebral Cortex, 2013, 23, 786-800.	1.6	153
78	Sparse temporally dynamic resting-state functional connectivity networks for early MCI identification. Brain Imaging and Behavior, 2016, 10, 342-356.	1.1	153
79	Estimating CT Image from MRI Data Using 3D Fully Convolutional Networks. Lecture Notes in Computer Science, 2016, 2016, 170-178.	1.0	151
80	Extraction of dynamic functional connectivity from brain grey matter and white matter for MCI classification. Human Brain Mapping, 2017, 38, 5019-5034.	1.9	151
81	Multi-task learning for segmentation and classification of tumors in 3D automated breast ultrasound images. Medical Image Analysis, 2021, 70, 101918.	7.0	151
82	ASDNet: Attention Based Semi-supervised Deep Networks for Medical Image Segmentation. Lecture Notes in Computer Science, 2018, , 370-378.	1.0	150
83	Adaptive Feature Selection Guided Deep Forest for COVID-19 Classification With Chest CT. IEEE Journal of Biomedical and Health Informatics, 2020, 24, 2798-2805.	3.9	149
84	Very High-Resolution Morphometry Using Mass-Preserving Deformations and HAMMER Elastic Registration. Neurolmage, 2003, 18, 28-41.	2.1	148
85	Spatial Patterns, Longitudinal Development, and Hemispheric Asymmetries of Cortical Thickness in Infants from Birth to 2 Years of Age. Journal of Neuroscience, 2015, 35, 9150-9162.	1.7	148
86	Domain Transfer Learning for MCI Conversion Prediction. IEEE Transactions on Biomedical Engineering, 2015, 62, 1805-1817.	2.5	148
87	LABEL: Pediatric brain extraction using learning-based meta-algorithm. NeuroImage, 2012, 62, 1975-1986.	2.1	147
88	The Synchronization within and Interaction between the Default and Dorsal Attention Networks in Early Infancy. Cerebral Cortex, 2013, 23, 594-603.	1.6	147
89	Detecting Anatomical Landmarks From Limited Medical Imaging Data Using Two-Stage Task-Oriented Deep Neural Networks. IEEE Transactions on Image Processing, 2017, 26, 4753-4764.	6.0	145
90	Multiple Kernel k-means with Incomplete Kernels. IEEE Transactions on Pattern Analysis and Machine Intelligence, 2019, 42, 1-1.	9.7	144

#	Article	IF	CITATIONS
91	Spatial normalization of diffusion tensor fields. Magnetic Resonance in Medicine, 2003, 50, 175-182.	1.9	143
92	Hippocampus Volume Loss Due to Chronic Heavy Drinking. Alcoholism: Clinical and Experimental Research, 2006, 30, 1866-1870.	1.4	141
93	Deep embedding convolutional neural network for synthesizing CT image from T1-Weighted MR image. Medical Image Analysis, 2018, 47, 31-44.	7.0	137
94	3D Auto-Context-Based Locality Adaptive Multi-Modality GANs for PET Synthesis. IEEE Transactions on Medical Imaging, 2019, 38, 1328-1339.	5.4	137
95	Benchmark on Automatic Six-Month-Old Infant Brain Segmentation Algorithms: The iSeg-2017 Challenge. IEEE Transactions on Medical Imaging, 2019, 38, 2219-2230.	5.4	136
96	3-D Fully Convolutional Networks for Multimodal Isointense Infant Brain Image Segmentation. IEEE Transactions on Cybernetics, 2019, 49, 1123-1136.	6.2	133
97	Multi-Channel 3D Deep Feature Learning for Survival Time Prediction of Brain Tumor Patients Using Multi-Modal Neuroimages. Scientific Reports, 2019, 9, 1103.	1.6	133
98	Automated detection and classification of thyroid nodules in ultrasound images using clinical-knowledge-guided convolutional neural networks. Medical Image Analysis, 2019, 58, 101555.	7.0	131
99	Resting-State Multi-Spectrum Functional Connectivity Networks for Identification of MCI Patients. PLoS ONE, 2012, 7, e37828.	1.1	127
100	High-Resolution Encoder–Decoder Networks for Low-Contrast Medical Image Segmentation. IEEE Transactions on Image Processing, 2020, 29, 461-475.	6.0	126
101	Integration of Network Topological and Connectivity Properties for Neuroimaging Classification. IEEE Transactions on Biomedical Engineering, 2014, 61, 576-589.	2.5	125
102	Computational neuroanatomy of baby brains: A review. NeuroImage, 2019, 185, 906-925.	2.1	125
103	Segmenting Lung Fields in Serial Chest Radiographs Using Both Population-Based and Patient-Specific Shape Statistics. IEEE Transactions on Medical Imaging, 2008, 27, 481-494.	5.4	124
104	Deep sparse multi-task learning for feature selection in Alzheimer's disease diagnosis. Brain Structure and Function, 2016, 221, 2569-2587.	1.2	124
105	Latent Representation Learning for Alzheimer's Disease Diagnosis With Incomplete Multi-Modality Neuroimaging and Genetic Data. IEEE Transactions on Medical Imaging, 2019, 38, 2411-2422.	5.4	124
106	Integration of temporal and spatial properties of dynamic connectivity networks for automatic diagnosis of brain disease. Medical Image Analysis, 2018, 47, 81-94.	7.0	123
107	Polyp detection during colonoscopy using a regression-based convolutional neural network with a tracker. Pattern Recognition, 2018, 83, 209-219.	5.1	122
108	Multivariate examination of brain abnormality using both structural and functional MRI. NeuroImage, 2007, 36, 1189-1199.	2.1	121

#	Article	IF	CITATIONS
109	Mapping Longitudinal Hemispheric Structural Asymmetries of the Human Cerebral Cortex From Birth to 2 Years of Age. Cerebral Cortex, 2014, 24, 1289-1300.	1.6	121
110	Alzheimer's Disease Diagnosis Using Landmark-Based Features From Longitudinal Structural MR Images. IEEE Journal of Biomedical and Health Informatics, 2017, 21, 1607-1616.	3.9	121
111	Deformable Image Registration Based on Similarity-Steered CNN Regression. Lecture Notes in Computer Science, 2017, 10433, 300-308.	1.0	121
112	Image registration by local histogram matching. Pattern Recognition, 2007, 40, 1161-1172.	5.1	120
113	Automatic segmentation of neonatal images using convex optimization and coupled level sets. NeuroImage, 2011, 58, 805-817.	2.1	120
114	Measuring Size and Shape of the Hippocampus in MR Images Using a Deformable Shape Model. NeuroImage, 2002, 15, 422-434.	2.1	119
115	Iterative multi-atlas-based multi-image segmentation with tree-based registration. NeuroImage, 2012, 59, 422-430.	2.1	119
116	Interleaved 3Dâ€ <scp>CNN</scp> s for joint segmentation of smallâ€volume structures in head and neck <scp>CT</scp> images. Medical Physics, 2018, 45, 2063-2075.	1.6	119
117	Axonal Fiber Terminations Concentrate on Gyri. Cerebral Cortex, 2012, 22, 2831-2839.	1.6	116
118	Deformable registration of cortical structures via hybrid volumetric and surface warping. NeuroImage, 2004, 22, 1790-1801.	2.1	114
119	Altered structural connectivity in neonates at genetic risk for schizophrenia: A combined study using morphological and white matter networks. NeuroImage, 2012, 62, 1622-1633.	2.1	114
120	Manifold regularized multitask feature learning for multimodality disease classification. Human Brain Mapping, 2015, 36, 489-507.	1.9	114
121	Anatomical Landmark Based Deep Feature Representation for MR Images in Brain Disease Diagnosis. IEEE Journal of Biomedical and Health Informatics, 2018, 22, 1476-1485.	3.9	114
122	White matter abnormalities revealed by diffusion tensor imaging in non-demented and demented HIV+ patients. NeuroImage, 2009, 47, 1154-1162.	2.1	113
123	Measuring the dynamic longitudinal cortex development in infants by reconstruction of temporally consistent cortical surfaces. NeuroImage, 2014, 90, 266-279.	2.1	113
124	Hierarchical fusion of features and classifier decisions for Alzheimer's disease diagnosis. Human Brain Mapping, 2014, 35, 1305-1319.	1.9	113
125	Hyper-connectivity of functional networks for brain disease diagnosis. Medical Image Analysis, 2016, 32, 84-100.	7.0	113
126	View-aligned hypergraph learning for Alzheimer's disease diagnosis with incomplete multi-modality data. Medical Image Analysis, 2017, 36, 123-134.	7.0	113

#	Article	IF	CITATIONS
127	Construction of 4D high-definition cortical surface atlases of infants: Methods and applications. Medical Image Analysis, 2015, 25, 22-36.	7.0	112
128	Unaffected Family Members and Schizophrenia Patients Share Brain Structure Patterns: A High-Dimensional Pattern Classification Study. Biological Psychiatry, 2008, 63, 118-124.	0.7	111
129	Estimating functional brain networks by incorporating a modularity prior. NeuroImage, 2016, 141, 399-407.	2.1	111
130	Structural and Maturational Covariance in Early Childhood Brain Development. Cerebral Cortex, 2017, 27, bhw022.	1.6	111
131	SharpMean: Groupwise registration guided by sharp mean image and tree-based registration. NeuroImage, 2011, 56, 1968-1981.	2.1	110
132	CLASSIC: Consistent Longitudinal Alignment and Segmentation for Serial Image Computing. NeuroImage, 2006, 30, 388-399.	2.1	109
133	Identifying Autism Spectrum Disorder With Multi-Site fMRI via Low-Rank Domain Adaptation. IEEE Transactions on Medical Imaging, 2020, 39, 644-655.	5.4	109
134	Spatial distribution and longitudinal development of deep cortical sulcal landmarks in infants. NeuroImage, 2014, 100, 206-218.	2.1	107
135	A generative probability model of joint label fusion for multi-atlas based brain segmentation. Medical Image Analysis, 2014, 18, 881-890.	7.0	107
136	Measuring temporal morphological changes robustly in brain MR images via 4-dimensional template warping. NeuroImage, 2004, 21, 1508-1517.	2.1	104
137	Topographical Information-Based High-Order Functional Connectivity and Its Application in Abnormality Detection forÂMild Cognitive Impairment. Journal of Alzheimer's Disease, 2016, 54, 1095-1112.	1.2	103
138	Hybrid High-order Functional Connectivity Networks Using Resting-state Functional MRI for Mild Cognitive Impairment Diagnosis. Scientific Reports, 2017, 7, 6530.	1.6	102
139	Classification of Structural Images via High-Dimensional Image Warping, Robust Feature Extraction, and SVM. Lecture Notes in Computer Science, 2005, 8, 1-8.	1.0	101
140	Strength and similarity guided group-level brain functional network construction for MCI diagnosis. Pattern Recognition, 2019, 88, 421-430.	5.1	101
141	An adaptive-focus deformable model using statistical and geometric information. IEEE Transactions on Pattern Analysis and Machine Intelligence, 2000, 22, 906-913.	9.7	100
142	ABSORB: Atlas building by self-organized registration and bundling. NeuroImage, 2010, 51, 1057-1070.	2.1	100
143	Adversarial learning for mono- or multi-modal registration. Medical Image Analysis, 2019, 58, 101545.	7.0	100
144	Deep Learning of Static and Dynamic Brain Functional Networks for Early MCI Detection. IEEE Transactions on Medical Imaging, 2020, 39, 478-487.	5.4	100

9

#	Article	IF	CITATIONS
145	Longitudinal clinical score prediction in Alzheimer's disease with soft-split sparse regression based random forest. Neurobiology of Aging, 2016, 46, 180-191.	1.5	99
146	Topological graph kernel on multiple thresholded functional connectivity networks for mild cognitive impairment classification. Human Brain Mapping, 2014, 35, 2876-2897.	1.9	98
147	Construction of multi-region-multi-reference atlases for neonatal brain MRI segmentation. NeuroImage, 2010, 51, 684-693.	2.1	96
148	Consistent reconstruction of cortical surfaces from longitudinal brain MR images. NeuroImage, 2012, 59, 3805-3820.	2.1	96
149	Integration of sparse multi-modality representation and anatomical constraint for isointense infant brain MR image segmentation. Neurolmage, 2014, 89, 152-164.	2.1	96
150	Inherent Structure-Based Multiview Learning With Multitemplate Feature Representation for Alzheimer's Disease Diagnosis. IEEE Transactions on Biomedical Engineering, 2016, 63, 1473-1482.	2.5	96
151	Multimodality image registration by maximization of quantitative–qualitative measure of mutual information. Pattern Recognition, 2008, 41, 285-298.	5.1	95
152	Hierarchical multi-atlas label fusion with multi-scale feature representation and label-specific patch partition. Neurolmage, 2015, 106, 34-46.	2.1	95
153	Learning-based deformable registration of MR brain images. IEEE Transactions on Medical Imaging, 2006, 25, 1145-1157.	5.4	93
154	Data-driven graph construction and graph learning: A review. Neurocomputing, 2018, 312, 336-351.	3.5	93
155	HER2, MET and FGFR2 oncogenic driver alterations define distinct molecular segments for targeted therapies in gastric carcinoma. British Journal of Cancer, 2014, 110, 1169-1178.	2.9	91
156	Multi-channel multi-scale fully convolutional network for 3D perivascular spaces segmentation in 7T MR images. Medical Image Analysis, 2018, 46, 106-117.	7.0	91
157	Resting-state functional MRI studies on infant brains: A decade of gap-filling efforts. NeuroImage, 2019, 185, 664-684.	2.1	91
158	Representation Learning: A Unified Deep Learning Framework for Automatic Prostate MR Segmentation. Lecture Notes in Computer Science, 2013, 16, 254-261.	1.0	91
159	ORBIT: A Multiresolution Framework for Deformable Registration of Brain Tumor Images. IEEE Transactions on Medical Imaging, 2008, 27, 1003-1017.	5.4	89
160	Viewâ€centralized multiâ€atlas classification for Alzheimer's disease diagnosis. Human Brain Mapping, 2015, 36, 1847-1865.	1.9	88
161	Weakly Supervised Segmentation of COVID19 Infection with Scribble Annotation on CT Images. Pattern Recognition, 2022, 122, 108341.	5.1	88
162	Deformable registration of brain tumor images via a statistical model of tumor-induced deformation. Medical Image Analysis, 2006, 10, 752-763.	7.0	87

#	Article	IF	CITATIONS
163	Neurodegenerative disease diagnosis using incomplete multi-modality data via matrix shrinkage and completion. NeuroImage, 2014, 91, 386-400.	2.1	87
164	Joint feature-sample selection and robust diagnosis of Parkinson's disease from MRI data. NeuroImage, 2016, 141, 206-219.	2.1	87
165	Sex differences in grey matter atrophy patterns among AD and aMCI patients: Results from ADNI. NeuroImage, 2011, 56, 890-906.	2.1	86
166	Deformable Image Registration Using a Cue-Aware Deep Regression Network. IEEE Transactions on Biomedical Engineering, 2018, 65, 1900-1911.	2.5	86
167	Robust Deformable-Surface-Based Skull-Stripping for Large-Scale Studies. Lecture Notes in Computer Science, 2011, 14, 635-642.	1.0	86
168	A Human Opsin-Related Gene That Encodes a Retinaldehyde-Binding Protein. Biochemistry, 1994, 33, 13117-13125.	1.2	85
169	Unsupervised Deep Feature Learning for Deformable Registration of MR Brain Images. Lecture Notes in Computer Science, 2013, 16, 649-656.	1.0	85
170	Canonical feature selection for joint regression and multi-class identification in Alzheimer's disease diagnosis. Brain Imaging and Behavior, 2016, 10, 818-828.	1.1	85
171	Connectivity strengthâ€weighted sparse group representationâ€based brain network construction for M <scp>Cl</scp> classification. Human Brain Mapping, 2017, 38, 2370-2383.	1.9	85
172	Simulating deformations of MR brain images for validation of atlas-based segmentation and registration algorithms. NeuroImage, 2006, 33, 855-866.	2.1	84
173	Spatiotemporal maturation patterns of murine brain quantified by diffusion tensor MRI and deformation-based morphometry. Proceedings of the National Academy of Sciences of the United States of America, 2005, 102, 6978-6983.	3.3	82
174	Developmental topography of cortical thickness during infancy. Proceedings of the National Academy of Sciences of the United States of America, 2019, 116, 15855-15860.	3.3	82
175	Regression Convolutional Neural Network for Automated Pediatric Bone Age Assessment From Hand Radiograph. IEEE Journal of Biomedical and Health Informatics, 2019, 23, 2030-2038.	3.9	82
176	Multimodal manifold-regularized transfer learning for MCI conversion prediction. Brain Imaging and Behavior, 2015, 9, 913-926.	1.1	81
177	Statistical representation of high-dimensional deformation fields with application to statistically constrained 3D warping. Medical Image Analysis, 2006, 10, 740-751.	7.0	80
178	Synthesizing Missing PET from MRI with Cycle-consistent Generative Adversarial Networks for Alzheimer's Disease Diagnosis. Lecture Notes in Computer Science, 2018, 11072, 455-463.	1.0	80
179	Automated morphometric study of brain variation in XXY males. NeuroImage, 2004, 23, 648-653.	2.1	79
180	Knowledge-Guided Robust MRI Brain Extraction for Diverse Large-Scale Neuroimaging Studies on Humans and Non-Human Primates. PLoS ONE, 2014, 9, e77810.	1.1	79

#	Article	IF	CITATIONS
181	Pelvic Organ Segmentation Using Distinctive Curve Guided Fully Convolutional Networks. IEEE Transactions on Medical Imaging, 2019, 38, 585-595.	5.4	79
182	Synergistic learning of lung lobe segmentation and hierarchical multi-instance classification for automated severity assessment of COVID-19 in CT images. Pattern Recognition, 2021, 113, 107828.	5.1	78
183	Non-diffeomorphic registration of brain tumor images by simulating tissue loss and tumor growth. NeuroImage, 2009, 46, 762-774.	2.1	77
184	Diagnosis of autism spectrum disorders using regional and interregional morphological features. Human Brain Mapping, 2014, 35, 3414-3430.	1.9	77
185	Remodeling Pearson's Correlation for Functional Brain Network Estimation and Autism Spectrum Disorder Identification. Frontiers in Neuroinformatics, 2017, 11, 55.	1.3	77
186	Deep Learning for Fast and Spatially Constrained Tissue Quantification From Highly Accelerated Data in Magnetic Resonance Fingerprinting. IEEE Transactions on Medical Imaging, 2019, 38, 2364-2374.	5.4	77
187	Structured sparsity regularized multiple kernel learning for Alzheimer's disease diagnosis. Pattern Recognition, 2019, 88, 370-382.	5.1	76
188	Deep CNN ensembles and suggestive annotations for infant brain MRI segmentation. Computerized Medical Imaging and Graphics, 2020, 79, 101660.	3.5	76
189	Registering Histologic and MR Images of Prostate for Image-based Cancer Detection. Academic Radiology, 2007, 14, 1367-1381.	1.3	75
190	iBEAT: A Toolbox for Infant Brain Magnetic Resonance Image Processing. Neuroinformatics, 2013, 11, 211-225.	1.5	75
191	Identification of infants at highâ€risk for autism spectrum disorder using multiparameter multiscale white matter connectivity networks. Human Brain Mapping, 2015, 36, 4880-4896.	1.9	75
192	Deep-Learning-Based Multi-Modal Fusion for Fast MR Reconstruction. IEEE Transactions on Biomedical Engineering, 2019, 66, 2105-2114.	2.5	75
193	RABBIT: Rapid alignment of brains by building intermediate templates. NeuroImage, 2009, 47, 1277-1287.	2.1	74
194	Convolutional Neural Network for Reconstruction of 7T-like Images from 3T MRI Using Appearance and Anatomical Features. Lecture Notes in Computer Science, 2016, , 39-47.	1.0	74
195	Spatial-Temporal Dependency Modeling and Network Hub Detection for Functional MRI Analysis via Convolutional-Recurrent Network. IEEE Transactions on Biomedical Engineering, 2020, 67, 2241-2252.	2.5	74
196	Deep Multi-Scale Mesh Feature Learning for Automated Labeling of Raw Dental Surfaces From 3D Intraoral Scanners. IEEE Transactions on Medical Imaging, 2020, 39, 2440-2450.	5.4	74
197	An affine-invariant active contour model (Al-snake) for model-based segmentation. Image and Vision Computing, 1998, 16, 135-146.	2.7	73
198	Diffusion tensor imaging based network analysis detects alterations of neuroconnectivity in patients with clinically early relapsingâ€remitting multiple sclerosis. Human Brain Mapping, 2013, 34, 3376-3391.	1.9	73

#	Article	IF	CITATIONS
199	A fully automatic AI system for tooth and alveolar bone segmentation from cone-beam CT images. Nature Communications, 2022, 13, 2096.	5.8	73
200	Development of cortical anatomical properties from early childhood to early adulthood. NeuroImage, 2013, 76, 216-224.	2.1	72
201	Label-aligned multi-task feature learning for multimodal classification of Alzheimer's disease and mild cognitive impairment. Brain Imaging and Behavior, 2016, 10, 1148-1159.	1.1	72
202	Semisupervised Tripled Dictionary Learning for Standard-Dose PET Image Prediction Using Low-Dose PET and Multimodal MRI. IEEE Transactions on Biomedical Engineering, 2017, 64, 569-579.	2.5	72
203	Conversion and time-to-conversion predictions of mild cognitive impairment using low-rank affinity pursuit denoising and matrix completion. Medical Image Analysis, 2018, 45, 68-82.	7.0	72
204	Sub-Network Kernels for Measuring Similarity of Brain Connectivity Networks in Disease Diagnosis. IEEE Transactions on Image Processing, 2018, 27, 2340-2353.	6.0	72
205	CT male pelvic organ segmentation using fully convolutional networks with boundary sensitive representation. Medical Image Analysis, 2019, 54, 168-178.	7.0	72
206	Severity assessment of COVID-19 using CT image features and laboratory indices. Physics in Medicine and Biology, 2021, 66, 035015.	1.6	72
207	Hierarchical Anatomical Brain Networks for MCI Prediction: Revisiting Volumetric Measures. PLoS ONE, 2011, 6, e21935.	1.1	72
208	Disrupted Brain Functional Network in Internet Addiction Disorder: A Resting-State Functional Magnetic Resonance Imaging Study. PLoS ONE, 2014, 9, e107306.	1.1	72
209	Accurate Segmentation of CT Male Pelvic Organs via Regression-Based Deformable Models and Multi-Task Random Forests. IEEE Transactions on Medical Imaging, 2016, 35, 1532-1543.	5.4	71
210	Diagnosis of Autism Spectrum Disorders Using Multi-Level High-Order Functional Networks Derived From Resting-State Functional MRI. Frontiers in Human Neuroscience, 2018, 12, 184.	1.0	71
211	Semi-Supervised Discriminative Classification Robust to Sample-Outliers and Feature-Noises. IEEE Transactions on Pattern Analysis and Machine Intelligence, 2019, 41, 515-522.	9.7	71
212	Context-guided fully convolutional networks for joint craniomaxillofacial bone segmentation and landmark digitization. Medical Image Analysis, 2020, 60, 101621.	7.0	71
213	A Mutual Multi-Scale Triplet Graph Convolutional Network for Classification of Brain Disorders Using Functional or Structural Connectivity. IEEE Transactions on Medical Imaging, 2021, 40, 1279-1289.	5.4	71
214	Optimized prostate biopsy via a statistical atlas of cancer spatial distribution. Medical Image Analysis, 2004, 8, 139-150.	7.0	70
215	First-year development of modules and hubs in infant brain functional networks. NeuroImage, 2019, 185, 222-235.	2.1	70
216	Segmenting CT prostate images using population and patientâ€specific statistics for radiotherapy. Medical Physics, 2010, 37, 4121-4132.	1.6	69

#	Article	IF	CITATIONS
217	TSegNet: An efficient and accurate tooth segmentation network on 3D dental model. Medical Image Analysis, 2021, 69, 101949.	7.0	69
218	4D Multi-Modality Tissue Segmentation of Serial Infant Images. PLoS ONE, 2012, 7, e44596.	1.1	67
219	Sparse Patch-Based Label Propagation for Accurate Prostate Localization in CT Images. IEEE Transactions on Medical Imaging, 2013, 32, 419-434.	5.4	67
220	Longitudinally guided level sets for consistent tissue segmentation of neonates. Human Brain Mapping, 2013, 34, 956-972.	1.9	66
221	Preserving Prostaglandin E2 Level Prevents Rejection of Implanted Allogeneic Mesenchymal Stem Cells and Restores Postinfarction Ventricular Function. Circulation, 2013, 128, S69-78.	1.6	66
222	Multimodal hyper-connectivity of functional networks using functionally-weighted LASSO for MCI classification. Medical Image Analysis, 2019, 52, 80-96.	7.0	66
223	A framework for predictive modeling of anatomical deformations. IEEE Transactions on Medical Imaging, 2001, 20, 836-843.	5.4	65
224	Connectome-scale assessments of structural and functional connectivity in MCI. Human Brain Mapping, 2014, 35, 2911-2923.	1.9	65
225	Characterization of U-shape streamline fibers: Methods and applications. Medical Image Analysis, 2014, 18, 795-807.	7.0	65
226	Multi-Domain Transfer Learning for Early Diagnosis of Alzheimer's Disease. Neuroinformatics, 2017, 15, 115-132.	1.5	65
227	Deep Adversarial Learning for Multi-Modality Missing Data Completion. , 2018, , .		65
228	Multi-site MRI harmonization via attention-guided deep domain adaptation for brain disorder identification. Medical Image Analysis, 2021, 71, 102076.	7.0	65
229	Diffusion Tensor Image Registration Using Tensor Geometry and Orientation Features. Lecture Notes in Computer Science, 2008, 11, 905-913.	1.0	65
230	Automated bone segmentation from dental CBCT images using patchâ€based sparse representation and convex optimization. Medical Physics, 2014, 41, 043503.	1.6	64
231	Matrix-Similarity Based Loss Function and Feature Selection for Alzheimer's Disease Diagnosis. , 2014, 2014, 3089-3096.		64
232	Multiâ€task diagnosis for autism spectrum disorders using multiâ€modality features: A multiâ€center study. Human Brain Mapping, 2017, 38, 3081-3097.	1.9	64
233	Reconstruction of 7T-Like Images From 3T MRI. IEEE Transactions on Medical Imaging, 2016, 35, 2085-2097.	5.4	63
234	Adversarial Similarity Network for Evaluating Image Alignment in Deep Learning Based Registration. Lecture Notes in Computer Science, 2018, 11070, 739-746.	1.0	63

#	Article	IF	CITATIONS
235	Multiâ€atlas based representations for Alzheimer's disease diagnosis. Human Brain Mapping, 2014, 35, 5052-5070.	1.9	62
236	Predicting standard-dose PET image from low-dose PET and multimodal MR images using mapping-based sparse representation. Physics in Medicine and Biology, 2016, 61, 791-812.	1.6	62
237	Deep Learning Based Inter-modality Image Registration Supervised by Intra-modality Similarity. Lecture Notes in Computer Science, 2018, 11046, 55-63.	1.0	62
238	Surface Vulnerability of Cerebral Cortex to Major Depressive Disorder. PLoS ONE, 2015, 10, e0120704.	1.1	62
239	Low-Rank Graph-Regularized Structured Sparse Regression for Identifying Genetic Biomarkers. IEEE Transactions on Big Data, 2017, 3, 405-414.	4.4	61
240	Volume-Based Analysis of 6-Month-Old Infant Brain MRI for Autism Biomarker Identification and Early Diagnosis. Lecture Notes in Computer Science, 2018, 11072, 411-419.	1.0	61
241	Weakly Supervised Deep Learning for Brain Disease Prognosis Using MRI and Incomplete Clinical Scores. IEEE Transactions on Cybernetics, 2019, 50, 1-12.	6.2	61
242	Dual-core steered non-rigid registration for multi-modal images via bi-directional image synthesis. Medical Image Analysis, 2017, 41, 18-31.	7.0	60
243	Environmental Influences on Infant Cortical Thickness and Surface Area. Cerebral Cortex, 2019, 29, 1139-1149.	1.6	60
244	Multi-modal latent space inducing ensemble SVM classifier for early dementia diagnosis with neuroimaging data. Medical Image Analysis, 2020, 60, 101630.	7.0	60
245	Diagnosis of Autism Spectrum Disorders Using Temporally Distinct Resting‣tate Functional Connectivity Networks. CNS Neuroscience and Therapeutics, 2016, 22, 212-219.	1.9	59
246	Affine-invariant image retrieval by correspondence matching of shapes. Image and Vision Computing, 1999, 17, 489-499.	2.7	58
247	Automated segmentation of dental CBCT image with prior-guided sequential random forests. Medical Physics, 2015, 43, 336-346.	1.6	58
248	Associations between Tumor Vascularity, Vascular Endothelial Growth Factor Expression and PET/MRI Radiomic Signatures in Primary Clear-Cell–Renal-Cell-Carcinoma: Proof-of-Concept Study. Scientific Reports, 2017, 7, 43356.	1.6	58
249	Joint prediction and time estimation of COVID-19 developing severe symptoms using chest CT scan. Medical Image Analysis, 2021, 67, 101824.	7.0	58
250	DeepDRiD: Diabetic Retinopathy—Grading and Image Quality Estimation Challenge. Patterns, 2022, 3, 100512.	3.1	58
251	Targeted Prostate Biopsy Using Statistical Image Analysis. IEEE Transactions on Medical Imaging, 2007, 26, 779-788.	5.4	57
252	Hierarchical Lung Field Segmentation With Joint Shape and Appearance Sparse Learning. IEEE Transactions on Medical Imaging, 2014, 33, 1761-1780.	5.4	57

#	Article	IF	CITATIONS
253	Artificial intelligence neuropathologist for glioma classification using deep learning on hematoxylin and eosin stained slide images and molecular markers. Neuro-Oncology, 2021, 23, 44-52.	0.6	57
254	Multiple-Network Classification of Childhood Autism Using Functional Connectivity Dynamics. Lecture Notes in Computer Science, 2014, 17, 177-184.	1.0	57
255	Deep Learning of Imaging Phenotype and Genotype for Predicting Overall Survival Time of Glioblastoma Patients. IEEE Transactions on Medical Imaging, 2020, 39, 2100-2109.	5.4	56
256	Hypergraph learning for identification of COVID-19 with CT imaging. Medical Image Analysis, 2021, 68, 101910.	7.0	56
257	Embryonic Stem Cell Grafting in Normal and Infarcted Myocardium: Serial Assessment with MR Imaging and PET Dual Detection. Radiology, 2009, 250, 821-829.	3.6	55
258	Hierarchical Vertex Regression-Based Segmentation of Head and Neck CT Images for Radiotherapy Planning. IEEE Transactions on Image Processing, 2018, 27, 923-937.	6.0	55
259	Test-Retest Reliability of "High-Order―Functional Connectivity in Young Healthy Adults. Frontiers in Neuroscience, 2017, 11, 439.	1.4	54
260	Segmentation and Classification in Digital Pathology for Glioma Research: Challenges and Deep Learning Approaches. Frontiers in Neuroscience, 2020, 14, 27.	1.4	54
261	Visualization of perivascular spaces in the human brain at 7 T: sequence optimization and morphology characterization. NeuroImage, 2016, 125, 895-902.	2.1	53
262	Domain-invariant interpretable fundus image quality assessment. Medical Image Analysis, 2020, 61, 101654.	7.0	53
263	Multi-Site Infant Brain Segmentation Algorithms: The iSeg-2019 Challenge. IEEE Transactions on Medical Imaging, 2021, 40, 1363-1376.	5.4	53
264	Cortical thickness and surface area in neonates at high risk for schizophrenia. Brain Structure and Function, 2016, 221, 447-461.	1.2	52
265	Largeâ€scale dynamic causal modeling of major depressive disorder based on restingâ€state functional magnetic resonance imaging. Human Brain Mapping, 2020, 41, 865-881.	1.9	52
266	A toolbox for brain network construction and classification (BrainNetClass). Human Brain Mapping, 2020, 41, 2808-2826.	1.9	52
267	Spatially-Constrained Fisher Representation for Brain Disease Identification With Incomplete Multi-Modal Neuroimages. IEEE Transactions on Medical Imaging, 2020, 39, 2965-2975.	5.4	52
268	Determining Correspondence in 3-D MR Brain Images Using Attribute Vectors as Morphological Signatures of Voxels. IEEE Transactions on Medical Imaging, 2004, 23, 1276-1291.	5.4	51
269	TIMER: Tensor Image Morphing for Elastic Registration. NeuroImage, 2009, 47, 549-563.	2.1	51
270	Longitudinal development of cortical thickness, folding, and fiber density networks in the first 2 years of life. Human Brain Mapping, 2014, 35, 3726-3737.	1.9	51

#	Article	IF	CITATIONS
271	Learning to Rank Atlases for Multiple-Atlas Segmentation. IEEE Transactions on Medical Imaging, 2014, 33, 1939-1953.	5.4	51
272	Task-Induced Pyramid and Attention GAN for Multimodal Brain Image Imputation and Classification in Alzheimer's Disease. IEEE Journal of Biomedical and Health Informatics, 2022, 26, 36-43.	3.9	51
273	Robust multi-label transfer feature learning for early diagnosis of Alzheimer's disease. Brain Imaging and Behavior, 2019, 13, 138-153.	1.1	50
274	Deep Learning and Medical Image Analysis for COVID-19 Diagnosis and Prediction. Annual Review of Biomedical Engineering, 2022, 24, 179-201.	5.7	50
275	A Computational Growth Model for Measuring Dynamic Cortical Development in the First Year of Life. Cerebral Cortex, 2012, 22, 2272-2284.	1.6	49
276	Prediction of standardâ€dose brain PET image by using MRI and lowâ€dose brain [ <sup>18</sup> F]FDG PET images. Medical Physics, 2015, 42, 5301-5309.	1.6	49
277	Temporally Constrained Group Sparse Learning for Longitudinal Data Analysis in Alzheimer's Disease. IEEE Transactions on Biomedical Engineering, 2017, 64, 238-249.	2.5	49
278	High-resolution 3D MR Fingerprinting using parallel imaging and deep learning. NeuroImage, 2020, 206, 116329.	2.1	49
279	Sparse Multiview Task-Centralized Ensemble Learning for ASD Diagnosis Based on Age- and Sex-Related Functional Connectivity Patterns. IEEE Transactions on Cybernetics, 2019, 49, 3141-3154.	6.2	48
280	Machine Learning in Orthodontics: <i>Introducing a 3d Auto-segmentation and Auto-landmark Finder of Cbct Images To Assess Maxillary Constriction in Unilateral Impacted Canine patients</i> . Angle Orthodontist, 2020, 90, 77-84.	1.1	48
281	Inferring Group-Wise Consistent Multimodal Brain Networks via Multi-View Spectral Clustering. IEEE Transactions on Medical Imaging, 2013, 32, 1576-1586.	5.4	47
282	Sâ€HAMMER: Hierarchical attributeâ€guided, symmetric diffeomorphic registration for MR brain images. Human Brain Mapping, 2014, 35, 1044-1060.	1.9	47
283	Automatic Craniomaxillofacial Landmark Digitization via Segmentation-Guided Partially-Joint Regression Forest Model and Multiscale Statistical Features. IEEE Transactions on Biomedical Engineering, 2016, 63, 1820-1829.	2.5	47
284	<scp>MRI</scp> â€based prostate cancer detection with highâ€level representation and hierarchical classification. Medical Physics, 2017, 44, 1028-1039.	1.6	47
285	Enhancing the representation of functional connectivity networks by fusing multiâ€view information for autism spectrum disorder diagnosis. Human Brain Mapping, 2019, 40, 833-854.	1.9	47
286	Prostate segmentation by sparse representation based classification. Medical Physics, 2012, 39, 6372-6387.	1.6	46
287	Automatic hippocampus segmentation of 7.0Tesla MR images by combining multiple atlases and auto-context models. NeuroImage, 2013, 83, 335-345.	2.1	46
288	Multi-Level Canonical Correlation Analysis for Standard-Dose PET Image Estimation. IEEE Transactions on Image Processing, 2016, 25, 3303-3315.	6.0	46

#	Article	IF	CITATIONS
289	Radiationâ€induced brain structural and functional abnormalities in presymptomatic phase and outcome prediction. Human Brain Mapping, 2018, 39, 407-427.	1.9	46
290	Initial experience in hybrid PET-MRI for evaluation of refractory focal onset epilepsy. Seizure: the Journal of the British Epilepsy Association, 2015, 31, 1-4.	0.9	45
291	An automated method for identifying an independent component analysis-based language-related resting-state network in brain tumor subjects for surgical planning. Scientific Reports, 2017, 7, 13769.	1.6	45
292	STRAINet: Spatially Varying sTochastic Residual AdversarIal Networks for MRI Pelvic Organ Segmentation. IEEE Transactions on Neural Networks and Learning Systems, 2019, 30, 1552-1564.	7.2	45
293	Altered Modular Organization of Structural Cortical Networks in Children with Autism. PLoS ONE, 2013, 8, e63131.	1.1	45
294	Featureâ€based groupwise registration by hierarchical anatomical correspondence detection. Human Brain Mapping, 2012, 33, 253-271.	1.9	44
295	Supervised Discriminative Group Sparse Representation for Mild Cognitive Impairment Diagnosis. Neuroinformatics, 2015, 13, 277-295.	1.5	44
296	Multi-Atlas Segmentation of MR Tumor Brain Images Using Low-Rank Based Image Recovery. IEEE Transactions on Medical Imaging, 2018, 37, 2224-2235.	5.4	44
297	Diagnosis of Autism Spectrum Disorder Using Central-Moment Features From Low- and High-Order Dynamic Resting-State Functional Connectivity Networks. Frontiers in Neuroscience, 2020, 14, 258.	1.4	44
298	Multi-Class ASD Classification Based on Functional Connectivity and Functional Correlation Tensor via Multi-Source Domain Adaptation and Multi-View Sparse Representation. IEEE Transactions on Medical Imaging, 2020, 39, 3137-3147.	5.4	44
299	Incomplete multi-modal representation learning for Alzheimer's disease diagnosis. Medical Image Analysis, 2021, 69, 101953.	7.0	44
300	Learning image context for segmentation of the prostate in CT-guided radiotherapy. Physics in Medicine and Biology, 2012, 57, 1283-1308.	1.6	43
301	Simultaneous Estimation of Low- and High-Order Functional Connectivity for Identifying Mild Cognitive Impairment. Frontiers in Neuroinformatics, 2018, 12, 3.	1.3	43
302	Genetic influences on neonatal cortical thickness and surface area. Human Brain Mapping, 2018, 39, 4998-5013.	1.9	43
303	Weighted graph regularized sparse brain network construction for MCI identification. Pattern Recognition, 2019, 90, 220-231.	5.1	43
304	Attention-Guided Hybrid Network for Dementia Diagnosis With Structural MR Images. IEEE Transactions on Cybernetics, 2022, 52, 1992-2003.	6.2	43
305	Synthesized 7T MRI from 3T MRI via deep learning in spatial and wavelet domains. Medical Image Analysis, 2020, 62, 101663.	7.0	43
306	Sparse Patch-Based Label Fusion for Multi-Atlas Segmentation. Lecture Notes in Computer Science, 2012, , 94-102.	1.0	43

#	Article	IF	CITATIONS
307	Brain-Wide Genome-Wide Association Study for Alzheimer's Disease via Joint Projection Learning and Sparse Regression Model. IEEE Transactions on Biomedical Engineering, 2019, 66, 165-175.	2.5	42
308	HF-UNet: Learning Hierarchically Inter-Task Relevance in Multi-Task U-Net for Accurate Prostate Segmentation in CT Images. IEEE Transactions on Medical Imaging, 2021, 40, 2118-2128.	5.4	42
309	Medical Image Synthesis via Deep Learning. Advances in Experimental Medicine and Biology, 2020, 1213, 23-44.	0.8	42
310	A Hopfield neural network for adaptive image segmentation: An active surface paradigm. Pattern Recognition Letters, 1997, 18, 37-48.	2.6	41
311	TPS-HAMMER: Improving HAMMER registration algorithm by soft correspondence matching and thin-plate splines based deformation interpolation. NeuroImage, 2010, 49, 2225-2233.	2.1	41
312	Automated Segmentation of 3D US Prostate Images Using Statistical Texture-Based Matching Method. Lecture Notes in Computer Science, 2003, , 688-696.	1.0	40
313	CENTS: Cortical enhanced neonatal tissue segmentation. Human Brain Mapping, 2011, 32, 382-396.	1.9	40
314	Improved image registration by sparse patch-based deformation estimation. Neurolmage, 2015, 105, 257-268.	2.1	40
315	Segmentation of Organs at Risk in thoracic CT images using a SharpMask architecture and Conditional Random Fields. , 2017, 2017, 1003-1006.		40
316	A novel multiple instance learning framework for COVID-19 severity assessment via data augmentation and self-supervised learning. Medical Image Analysis, 2021, 69, 101978.	7.0	40
317	Denoising magnetic resonance images using collaborative non-local means. Neurocomputing, 2016, 177, 215-227.	3.5	39
318	Leveraging Coupled Interaction for Multimodal Alzheimer's Disease Diagnosis. IEEE Transactions on Neural Networks and Learning Systems, 2020, 31, 186-200.	7.2	39
319	Toward a Better Estimation of Functional Brain Network for Mild Cognitive Impairment Identification: A Transfer Learning View. IEEE Journal of Biomedical and Health Informatics, 2020, 24, 1160-1168.	3.9	39
320	DesigningÂweightedÂcorrelationÂkernelsÂinÂconvolutional neural networks for functional connectivity based brain disease diagnosis. Medical Image Analysis, 2020, 63, 101709.	7.0	39
321	Harmonization of Infant Cortical Thickness Using Surface-to-Surface Cycle-Consistent Adversarial Networks. Lecture Notes in Computer Science, 2019, 11767, 475-483.	1.0	39
322	Adaptive rectification based adversarial network with spectrum constraint for high-quality PET image synthesis. Medical Image Analysis, 2022, 77, 102335.	7.0	39
323	Domain Transfer Learning for MCI Conversion Prediction. Lecture Notes in Computer Science, 2012, 15, 82-90.	1.0	38
324	Segmentation of perivascular spaces in 7 T MR image using auto-context model with orientation-normalized features. NeuroImage, 2016, 134, 223-235.	2.1	38

#	Article	IF	CITATIONS
325	7Tâ€guided superâ€resolution of 3T MRI. Medical Physics, 2017, 44, 1661-1677.	1.6	38
326	Dilated Dense U-Net for Infant Hippocampus Subfield Segmentation. Frontiers in Neuroinformatics, 2019, 13, 30.	1.3	38
327	Automatic Skull Stripping of Rat and Mouse Brain MRI Data Using U-Net. Frontiers in Neuroscience, 2020, 14, 568614.	1.4	38
328	Hypercortisolism in Alcohol Dependence and Its Relation to Hippocampal Volume Loss. Journal of Studies on Alcohol and Drugs, 2006, 67, 861-867.	2.4	37
329	Hierarchical Patch-Based Sparse Representation—A New Approach for Resolution Enhancement of 4D-CT Lung Data. IEEE Transactions on Medical Imaging, 2012, 31, 1993-2005.	5.4	37
330	Spherical U-Net on Cortical Surfaces: Methods and Applications. Lecture Notes in Computer Science, 2019, 11492, 855-866.	1.0	37
331	Overall survival time prediction for high-grade glioma patients based on large-scale brain functional networks. Brain Imaging and Behavior, 2019, 13, 1333-1351.	1.1	37
332	Review and Prospect: Artificial Intelligence in Advanced Medical Imaging. Frontiers in Radiology, 2021, 1, .	1.2	37
333	Hierarchical unbiased graph shrinkage (HUGS): A novel groupwise registration for large data set. Neurolmage, 2014, 84, 626-638.	2.1	36
334	Non-Negative Spherical Deconvolution (NNSD) for estimation of fiber Orientation Distribution Function in single-/multi-shell diffusion MRI. NeuroImage, 2014, 101, 750-764.	2.1	36
335	Discriminative multi-task feature selection for multi-modality classification of Alzheimer's disease. Brain Imaging and Behavior, 2016, 10, 739-749.	1.1	36
336	Reduced White Matter Integrity in Antisocial Personality Disorder: A Diffusion Tensor Imaging Study. Scientific Reports, 2017, 7, 43002.	1.6	36
337	Region-Adaptive Deformable Registration of CT/MRI Pelvic Images via Learning-Based Image Synthesis. IEEE Transactions on Image Processing, 2018, 27, 3500-3512.	6.0	36
338	Multi-task exclusive relationship learning for alzheimer's disease progression prediction with longitudinal data. Medical Image Analysis, 2019, 53, 111-122.	7.0	36
339	The emergence of a functionally flexible brain during early infancy. Proceedings of the National Academy of Sciences of the United States of America, 2020, 117, 23904-23913.	3.3	36
340	Constrained Sparse Functional Connectivity Networks for MCI Classification. Lecture Notes in Computer Science, 2012, 15, 212-219.	1.0	36
341	SPHERE: SPherical Harmonic Elastic REgistration of HARDI data. NeuroImage, 2011, 55, 545-556.	2.1	35
342	Subclass-based multi-task learning for Alzheimer's disease diagnosis. Frontiers in Aging Neuroscience, 2014, 6, 168.	1.7	35

#	Article	IF	CITATIONS
343	Structured Learning for 3-D Perivascular Space Segmentation Using Vascular Features. IEEE Transactions on Biomedical Engineering, 2017, 64, 2803-2812.	2.5	35
344	Groupwise registration based on hierarchical image clustering and atlas synthesis. Human Brain Mapping, 2010, 31, 1128-1140.	1.9	34
345	Neonatal atlas construction using sparse representation. Human Brain Mapping, 2014, 35, 4663-4677.	1.9	34
346	Multi-modality Canonical Feature Selection for Alzheimer's Disease Diagnosis. Lecture Notes in Computer Science, 2014, 17, 162-169.	1.0	34
347	Simultaneous and consistent labeling of longitudinal dynamic developing cortical surfaces in infants. Medical Image Analysis, 2014, 18, 1274-1289.	7.0	34
348	Locally-constrained boundary regression for segmentation of prostate and rectum in the planning CT images. Medical Image Analysis, 2015, 26, 345-356.	7.0	34
349	Deep Chronnectome Learning via Full Bidirectional Long Short-Term Memory Networks for MCI Diagnosis. Lecture Notes in Computer Science, 2018, 11072, 249-257.	1.0	34
350	Functional Brain Network Estimation With Time Series Self-Scrubbing. IEEE Journal of Biomedical and Health Informatics, 2019, 23, 2494-2504.	3.9	34
351	Cascaded MultiTask 3-D Fully Convolutional Networks for Pancreas Segmentation. IEEE Transactions on Cybernetics, 2021, 51, 2153-2165.	6.2	34
352	Intermediate templates guided groupwise registration of diffusion tensor images. NeuroImage, 2011, 54, 928-939.	2.1	33
353	Consistent Spatial-Temporal Longitudinal Atlas Construction for Developing Infant Brains. IEEE Transactions on Medical Imaging, 2016, 35, 2568-2577.	5.4	33
354	Identification of progressive mild cognitive impairment patients using incomplete longitudinal MRI scans. Brain Structure and Function, 2016, 221, 3979-3995.	1.2	33
355	Deep Multi-task Multi-channel Learning for Joint Classification and Regression of Brain Status. Lecture Notes in Computer Science, 2017, 10435, 3-11.	1.0	33
356	Multi-Hypergraph Learning for Incomplete Multimodality Data. IEEE Journal of Biomedical and Health Informatics, 2018, 22, 1197-1208.	3.9	33
357	Disease-Image-Specific Learning for Diagnosis-Oriented Neuroimage Synthesis With Incomplete Multi-Modality Data. IEEE Transactions on Pattern Analysis and Machine Intelligence, 2022, 44, 6839-6853.	9.7	33
358	A review of deep learning-based three-dimensional medical image registration methods. Quantitative Imaging in Medicine and Surgery, 2021, 11, 4895-4916.	1.1	33
359	Spherical Deformable U-Net: Application to Cortical Surface Parcellation and Development Prediction. IEEE Transactions on Medical Imaging, 2021, 40, 1217-1228.	5.4	33
360	Multiscale adaptive generalized estimating equations for longitudinal neuroimaging data. NeuroImage, 2013, 72, 91-105.	2.1	32

#	Article	IF	CITATIONS
361	Sparse Multivariate Autoregressive Modeling for Mild Cognitive Impairment Classification. Neuroinformatics, 2014, 12, 455-469.	1.5	32
362	Spatiotemporal patterns of cortical fiber density in developing infants, and their relationship with cortical thickness. Human Brain Mapping, 2015, 36, 5183-5195.	1.9	32
363	Early Diagnosis of Autism Disease by Multi-channel CNNs. Lecture Notes in Computer Science, 2018, 11046, 303-309.	1.0	32
364	Multi-View Spatial Aggregation Framework for Joint Localization and Segmentation of Organs at Risk in Head and Neck CT Images. IEEE Transactions on Medical Imaging, 2020, 39, 2794-2805.	5.4	32
365	Diverse data augmentation for learning image segmentation with cross-modality annotations. Medical Image Analysis, 2021, 71, 102060.	7.0	32
366	Multi-stage Diagnosis of Alzheimer's Disease with Incomplete Multimodal Data viaÂMulti-task Deep Learning. Lecture Notes in Computer Science, 2017, 10553, 160-168.	1.0	32
367	Semi-Supervised Deep Transfer Learning for Benign-Malignant Diagnosis of Pulmonary Nodules in Chest CT Images. IEEE Transactions on Medical Imaging, 2022, 41, 771-781.	5.4	32
368	Registration of longitudinal brain image sequences with implicit template and spatial–temporal heuristics. NeuroImage, 2012, 59, 404-421.	2.1	31
369	Segmenting Hippocampus from Infant Brains by Sparse Patch Matching with Deep-Learned Features. Lecture Notes in Computer Science, 2014, 17, 308-315.	1.0	31
370	Graph-guided joint prediction of class label and clinical scores for the Alzheimer's disease. Brain Structure and Function, 2016, 221, 3787-3801.	1.2	31
371	A Hierarchical Feature and Sample Selection Framework and Its Application for Alzheimer's Disease Diagnosis. Scientific Reports, 2017, 7, 45269.	1.6	31
372	Hierarchical High-Order Functional Connectivity Networks and Selective Feature Fusion for MCI Classification. Neuroinformatics, 2017, 15, 271-284.	1.5	31
373	Robust multi-atlas label propagation by deep sparse representation. Pattern Recognition, 2017, 63, 511-517.	5.1	31
374	Multi-View Missing Data Completion. IEEE Transactions on Knowledge and Data Engineering, 2018, 30, 1296-1309.	4.0	31
375	Integrative radiomics expression predicts molecular subtypes of primary clear cell renal cell carcinoma. Clinical Radiology, 2018, 73, 782-791.	0.5	31
376	Construction of 4D infant cortical surface atlases with sharp folding patterns via spherical patchâ€based groupâ€wise sparse representation. Human Brain Mapping, 2019, 40, 3860-3880.	1.9	31
377	Fetal cortical surface atlas parcellation based on growth patterns. Human Brain Mapping, 2019, 40, 3881-3899.	1.9	31
378	Integrative analysis of multi-dimensional imaging genomics data for Alzheimer's disease prediction. Frontiers in Aging Neuroscience, 2014, 6, 260.	1.7	30

#	Article	IF	CITATIONS
379	Predict brain MR image registration via sparse learning of appearance and transformation. Medical Image Analysis, 2015, 20, 61-75.	7.0	30
380	Deep Learning in Diagnosis of Brain Disorders. Trends in Augmentation of Human Performance, 2015, , 203-213.	0.4	30
381	Manifold Regularized Multi-Task Feature Selection for Multi-Modality Classification in Alzheimer's Disease. Lecture Notes in Computer Science, 2013, 16, 275-283.	1.0	30
382	Attribute vector guided groupwise registration. NeuroImage, 2010, 50, 1485-1496.	2.1	29
383	A Feature-Based Learning Framework for Accurate Prostate Localization in CT Images. IEEE Transactions on Image Processing, 2012, 21, 3546-3559.	6.0	29
384	A General Fast Registration Framework by Learning Deformation–Appearance Correlation. IEEE Transactions on Image Processing, 2012, 21, 1823-1833.	6.0	29
385	Enhancement of Perivascular Spaces in 7 T MR Image using Haar Transform of Non-local Cubes and Block-matching Filtering. Scientific Reports, 2017, 7, 8569.	1.6	29
386	Adversarial Confidence Learning for Medical Image Segmentation and Synthesis. International Journal of Computer Vision, 2020, 128, 2494-2513.	10.9	29
387	Prediction of 7â€year's conversion from subjective cognitive decline to mild cognitive impairment. Human Brain Mapping, 2021, 42, 192-203.	1.9	29
388	Outcome Prediction for Patient with High-Grade Gliomas from Brain Functional and Structural Networks. Lecture Notes in Computer Science, 2016, 9901, 26-34.	1.0	29
389	F-TIMER: Fast Tensor Image Morphing for Elastic Registration. IEEE Transactions on Medical Imaging, 2010, 29, 1192-1203.	5.4	28
390	Structured Sparse Kernel Learning for Imaging Genetics Based Alzheimer's Disease Diagnosis. Lecture Notes in Computer Science, 2016, 9901, 70-78.	1.0	28
391	Longitudinally Guided Super-Resolution of Neonatal Brain Magnetic Resonance Images. IEEE Transactions on Cybernetics, 2019, 49, 662-674.	6.2	28
392	Morphology of perivascular spaces and enclosed blood vessels in young to middle-aged healthy adults at 7T: Dependences on age, brain region, and breathing gas. NeuroImage, 2020, 218, 116978.	2.1	28
393	Spatial Transformation of DWI Data Using Non-Negative Sparse Representation. IEEE Transactions on Medical Imaging, 2012, 31, 2035-2049.	5.4	27
394	Application of neuroanatomical features to tractography clustering. Human Brain Mapping, 2013, 34, 2089-2102.	1.9	27
395	Prostate Segmentation in CT Images via Spatial-Constrained Transductive Lasso. , 2013, , .		27
396	Predicting infant cortical surface development using a 4D varifold-based learning framework and local topography-based shape morphing. Medical Image Analysis, 2016, 28, 1-12.	7.0	27

#	Article	IF	CITATIONS
397	Gyral net: A new representation of cortical folding organization. Medical Image Analysis, 2017, 42, 14-25.	7.0	27
398	Automatic brain labeling via multi-atlas guided fully convolutional networks. Medical Image Analysis, 2019, 51, 157-168.	7.0	27
399	Disentangled-Multimodal Adversarial Autoencoder: Application to Infant Age Prediction With Incomplete Multimodal Neuroimages. IEEE Transactions on Medical Imaging, 2020, 39, 4137-4149.	5.4	27
400	MCI Identification by Joint Learning on Multiple MRI Data. Lecture Notes in Computer Science, 2015, 9350, 78-85.	1.0	27
401	Multi-view Classification for Identification of Alzheimer's Disease. Lecture Notes in Computer Science, 2015, 9352, 255-262.	1.0	27
402	Joint Craniomaxillofacial Bone Segmentation and Landmark Digitization by Context-Guided Fully Convolutional Networks. Lecture Notes in Computer Science, 2017, 10434, 720-728.	1.0	27
403	Semi-Automatic Segmentation of Prostate in CT Images via Coupled Feature Representation and Spatial-Constrained Transductive Lasso. IEEE Transactions on Pattern Analysis and Machine Intelligence, 2015, 37, 2286-2303.	9.7	26
404	Automatic labeling of MR brain images by hierarchical learning of atlas forests. Medical Physics, 2016, 43, 1175-1186.	1.6	26
405	Mapping hemispheric asymmetries of the macaque cerebral cortex during early brain development. Human Brain Mapping, 2020, 41, 95-106.	1.9	26
406	Submillimeter MR fingerprinting using deep learning–based tissue quantification. Magnetic Resonance in Medicine, 2020, 84, 579-591.	1.9	26
407	Cross-Site Severity Assessment of COVID-19 From CT Images via Domain Adaptation. IEEE Transactions on Medical Imaging, 2022, 41, 88-102.	5.4	26
408	Disease-Image Specific Generative Adversarial Network for Brain Disease Diagnosis with Incomplete Multi-modal Neuroimages. Lecture Notes in Computer Science, 2019, , 137-145.	1.0	26
409	A transversal approach for patch-based label fusion via matrix completion. Medical Image Analysis, 2015, 24, 135-148.	7.0	25
410	Reduced cortical thickness and increased surface area in antisocial personality disorder. Neuroscience, 2016, 337, 143-152.	1.1	25
411	Sparse Multi-Response Tensor Regression for Alzheimer's Disease Study With Multivariate Clinical Assessments. IEEE Transactions on Medical Imaging, 2016, 35, 1927-1936.	5.4	25
412	Feature fusion via hierarchical supervised local CCA for diagnosis of autism spectrum disorder. Brain Imaging and Behavior, 2017, 11, 1050-1060.	1.1	25
413	Tumor Tissue Detection using Blood-Oxygen-Level-Dependent Functional MRI based on Independent Component Analysis. Scientific Reports, 2018, 8, 1223.	1.6	25
414	Multi-Label Nonlinear Matrix Completion With Transductive Multi-Task Feature Selection for Joint MGMT and IDH1 Status Prediction of Patient With High-Grade Gliomas. IEEE Transactions on Medical Imaging, 2018, 37, 1775-1787.	5.4	25

#	Article	IF	CITATIONS
415	Robust brain ROI segmentation by deformation regression and deformable shape model. Medical Image Analysis, 2018, 43, 198-213.	7.0	25
416	Exploring folding patterns of infant cerebral cortex based on multi-view curvature features: Methods and applications. NeuroImage, 2019, 185, 575-592.	2.1	25
417	A New Multi-Atlas Registration Framework for Multimodal Pathological Images Using Conventional Monomodal Normal Atlases. IEEE Transactions on Image Processing, 2019, 28, 2293-2304.	6.0	25
418	Cortical Structure and Cognition in Infants and Toddlers. Cerebral Cortex, 2020, 30, 786-800.	1.6	25
419	Individual identification and individual variability analysis based on cortical folding features in developing infant singletons and twins. Human Brain Mapping, 2020, 41, 1985-2003.	1.9	25
420	Consistent Estimation of Cardiac Motions by 4D Image Registration. Lecture Notes in Computer Science, 2005, 8, 902-910.	1.0	25
421	High-Order Graph Matching Based Feature Selection for Alzheimer's Disease Identification. Lecture Notes in Computer Science, 2013, 16, 311-318.	1.0	25
422	Two-Stage Mesh Deep Learning for Automated Tooth Segmentation and Landmark Localization on 3D Intraoral Scans. IEEE Transactions on Medical Imaging, 2022, 41, 3158-3166.	5.4	25
423	Semi-supervised multimodal classification of alzheimer's disease. , 2011, , .		24
424	Multi-Site Harmonization of Diffusion MRI Data via Method of Moments. IEEE Transactions on Medical Imaging, 2019, 38, 1599-1609.	5.4	24
425	Treatment-naÃ⁻ve first episode depression classification based on high-order brain functional network. Journal of Affective Disorders, 2019, 256, 33-41.	2.0	24
426	Hippocampus Radiomic Biomarkers for the Diagnosis of Amnestic Mild Cognitive Impairment: A Machine Learning Method. Frontiers in Aging Neuroscience, 2019, 11, 323.	1.7	24
427	Multi-task prediction of infant cognitive scores from longitudinal incomplete neuroimaging data. NeuroImage, 2019, 185, 783-792.	2.1	24
428	Learning longitudinal classification-regression model for infant hippocampus segmentation. Neurocomputing, 2020, 391, 191-198.	3.5	24
429	Mitigating gyral bias in cortical tractography via asymmetric fiber orientation distributions. Medical Image Analysis, 2020, 59, 101543.	7.0	24
430	One-Shot Generative Adversarial Learning for MRI Segmentation of Craniomaxillofacial Bony Structures. IEEE Transactions on Medical Imaging, 2020, 39, 787-796.	5.4	24
431	Edge-preserving MRI image synthesis via adversarial network with iterative multi-scale fusion. Neurocomputing, 2021, 452, 63-77.	3.5	24
432	Triplet Graph Convolutional Network for Multi-scale Analysis of Functional Connectivity Using Functional MRI. Lecture Notes in Computer Science, 2019, , 70-78.	1.0	24

#	Article	IF	CITATIONS
433	Learning Image Context for Segmentation of Prostate in CT-Guided Radiotherapy. Lecture Notes in Computer Science, 2011, 14, 570-578.	1.0	24
434	Coregistration of Magnetic Resonance and Single Photon Emission Computed Tomography Images for Noninvasive Localization of Stem Cells Grafted in the Infarcted Rat Myocardium. Molecular Imaging and Biology, 2007, 9, 24-31.	1.3	23
435	Fast image registration by hierarchical soft correspondence detection. Pattern Recognition, 2009, 42, 954-961.	5.1	23
436	A novel framework for longitudinal atlas construction with groupwise registration of subject image sequences. Neurolmage, 2012, 59, 1275-1289.	2.1	23
437	Joint Coupled-Feature Representation and Coupled Boosting for AD Diagnosis. , 2014, 2014, 2721-2728.		23
438	MRIâ€based prostate volumeâ€adjusted prostateâ€specific antigen in the diagnosis of prostate cancer. Journal of Magnetic Resonance Imaging, 2015, 42, 1733-1739.	1.9	23
439	Multilevel Deficiency of White Matter Connectivity Networks in Alzheimer's Disease: A Diffusion MRI Study with DTI and HARDI Models. Neural Plasticity, 2016, 2016, 1-14.	1.0	23
440	Joint prediction of longitudinal development of cortical surfaces and white matter fibers from neonatal MRI. NeuroImage, 2017, 152, 411-424.	2.1	23
441	Craniomaxillofacial Bony Structures Segmentation from MRI with Deep-Supervision Adversarial Learning. Lecture Notes in Computer Science, 2018, 11073, 720-727.	1.0	23
442	A Novel Deep Learning Framework on Brain Functional Networks for Early MCI Diagnosis. Lecture Notes in Computer Science, 2018, 11072, 293-301.	1.0	23
443	Ultra-Fast T2-Weighted MR Reconstruction Using Complementary T1-Weighted Information. Lecture Notes in Computer Science, 2018, 11070, 215-223.	1.0	23
444	Fully automatic segmentation of paraspinal muscles from 3D torso CT images via multi-scale iterative random forest classifications. International Journal of Computer Assisted Radiology and Surgery, 2018, 13, 1697-1706.	1.7	23
445	Denoising of Diffusion MRI Data via Graph Framelet Matching in x-q Space. IEEE Transactions on Medical Imaging, 2019, 38, 2838-2848.	5.4	23
446	3D Transformer-GAN for High-Quality PET Reconstruction. Lecture Notes in Computer Science, 2021, , 276-285.	1.0	23
447	Interactive prostate segmentation using atlasâ€guided semiâ€supervised learning and adaptive feature selection. Medical Physics, 2014, 41, 111715.	1.6	22
448	Reveal Consistent Spatial-Temporal Patterns from Dynamic Functional Connectivity for Autism Spectrum Disorder Identification. Lecture Notes in Computer Science, 2016, 9900, 106-114.	1.0	22
449	Concatenated spatially-localized random forests for hippocampus labeling in adult and infant MR brain images. Neurocomputing, 2017, 229, 3-12.	3.5	22
450	Evaluation of PET/MRI for Tumor Volume Delineation for Head and Neck Cancer. Frontiers in Oncology, 2017, 7, 8.	1.3	22

#	Article	IF	CITATIONS
451	Difficulty-Aware Attention Network with Confidence Learning for Medical Image Segmentation. Proceedings of the AAAI Conference on Artificial Intelligence, 2019, 33, 1085-1092.	3.6	22
452	Enhancement of Perivascular Spaces Using Densely Connected Deep Convolutional Neural Network. IEEE Access, 2019, 7, 18382-18391.	2.6	22
453	Modeling Hierarchical Brain Networks via Volumetric Sparse Deep Belief Network. IEEE Transactions on Biomedical Engineering, 2020, 67, 1739-1748.	2.5	22
454	Guest Editorial: Special Issue on Imaging-Based Diagnosis of COVID-19. IEEE Transactions on Medical Imaging, 2020, 39, 2569-2571.	5.4	22
455	RCA-U-Net: Residual Channel Attention U-Net for Fast Tissue Quantification in Magnetic Resonance Fingerprinting. Lecture Notes in Computer Science, 2019, 11766, 101-109.	1.0	22
456	Multiview Feature Learning With Multiatlas-Based Functional Connectivity Networks for MCI Diagnosis. IEEE Transactions on Cybernetics, 2022, 52, 6822-6833.	6.2	22
457	Lung Nodule Growth Analysis from 3D CT Data with a Coupled Segmentation and Registration Framework. , 2007, , .		21
458	Estimating the 4D respiratory lung motion by spatiotemporal registration and superâ€resolution image reconstruction. Medical Physics, 2013, 40, 031710.	1.6	21
459	Identifying Informative Imaging Biomarkers via Tree Structured Sparse Learning for AD Diagnosis. Neuroinformatics, 2014, 12, 381-394.	1.5	21
460	Collaborative regression-based anatomical landmark detection. Physics in Medicine and Biology, 2015, 60, 9377-9401.	1.6	21
461	Robust anatomical landmark detection with application to MR brain image registration. Computerized Medical Imaging and Graphics, 2015, 46, 277-290.	3.5	21
462	Early Diagnosis of Alzheimer's Disease by Joint Feature Selection and Classification on Temporally Structured Support Vector Machine. Lecture Notes in Computer Science, 2016, 9900, 264-272.	1.0	21
463	Learning non-linear patch embeddings with neural networks for label fusion. Medical Image Analysis, 2018, 44, 143-155.	7.0	21
464	Registration-Free Infant Cortical Surface Parcellation Using Deep Convolutional Neural Networks. Lecture Notes in Computer Science, 2018, 11072, 672-680.	1.0	21
465	Noise reduction in diffusion MRI using non-local self-similar information in joint <mml:math xmlns:mml="http://www.w3.org/1998/Math/MathML" altimg="si1.gif" overflow="scroll"&gt;<mml:mrow><mml:mi>x</mml:mi><mml:mo>â^</mml:mo><mml:mi>q</mml:mi>Medical Image Analysis. 2019. 53. 79-94.</mml:mrow></mml:math 	v>7:0 v> <td>nath&gt;space.</td>	nath>space.
466	Learning MRI artefact removal with unpaired data. Nature Machine Intelligence, 2021, 3, 60-67.	8.3	21
467	Structure-Driven Unsupervised Domain Adaptation for Cross-Modality Cardiac Segmentation. IEEE Transactions on Medical Imaging, 2021, 40, 3604-3616.	5.4	21
468	A Novel Multi-relation Regularization Method for Regression and Classification in AD Diagnosis. Lecture Notes in Computer Science, 2014, 17, 401-408.	1.0	21

#	Article	IF	CITATIONS
469	Brain Connectivity Hyper-Network for MCI Classification. Lecture Notes in Computer Science, 2014, 17, 724-732.	1.0	21
470	PopTract: Population-Based Tractography. IEEE Transactions on Medical Imaging, 2011, 30, 1829-1840.	5.4	20
471	Semi-Supervised Multimodal Relevance Vector Regression Improves Cognitive Performance Estimation from Imaging and Biological Biomarkers. Neuroinformatics, 2013, 11, 339-353.	1.5	20
472	Robust Anatomical Landmark Detection for MR Brain Image Registration. Lecture Notes in Computer Science, 2014, 17, 186-193.	1.0	20
473	Multi-atlas and Multi-modal Hippocampus Segmentation for Infant MR Brain Images by Propagating Anatomical Labels on Hypergraph. Lecture Notes in Computer Science, 2015, 9467, 188-196.	1.0	20
474	Abnormal Changes of Brain Cortical Anatomy and the Association with Plasma MicroRNA107 Level in Amnestic Mild Cognitive Impairment. Frontiers in Aging Neuroscience, 2016, 8, 112.	1.7	20
475	Multi-Tissue Decomposition of Diffusion MRI Signals via LO Sparse-Group Estimation. IEEE Transactions on Image Processing, 2016, 25, 1-1.	6.0	20
476	Multi-task feature selection via supervised canonical graph matching for diagnosis of autism spectrum disorder. Brain Imaging and Behavior, 2016, 10, 33-40.	1.1	20
477	Segmentation of Craniomaxillofacial Bony Structures from MRI with a 3D Deep-Learning Based Cascade Framework. Lecture Notes in Computer Science, 2017, 10541, 266-273.	1.0	20
478	Anatomyâ€guided joint tissue segmentation and topological correction for 6â€month infant brain MRI with risk of autism. Human Brain Mapping, 2018, 39, 2609-2623.	1.9	20
479	Improving Sparsity and Modularity of High-Order Functional Connectivity Networks for MCI and ASD Identification. Frontiers in Neuroscience, 2018, 12, 959.	1.4	20
480	Semi-supervised learning for pelvic MR image segmentation based on multi-task residual fully convolutional networks. , 2018, 2018, 885-888.		20
481	Foreground Fisher Vector: Encoding Class-Relevant Foreground to Improve Image Classification. IEEE Transactions on Image Processing, 2019, 28, 4716-4729.	6.0	20
482	SLIR: Synthesis, localization, inpainting, and registration for image-guided thermal ablation of liver tumors. Medical Image Analysis, 2020, 65, 101763.	7.0	20
483	Interactive medical image segmentation via a point-based interaction. Artificial Intelligence in Medicine, 2021, 111, 101998.	3.8	20
484	Multi-Task Weakly-Supervised Attention Network for Dementia Status Estimation With Structural MRI. IEEE Transactions on Neural Networks and Learning Systems, 2022, 33, 4056-4068.	7.2	20
485	MeshSNet: Deep Multi-scale Mesh Feature Learning for End-to-End Tooth Labeling on 3D Dental Surfaces. Lecture Notes in Computer Science, 2019, , 837-845.	1.0	20
486	De-enhancing the Dynamic Contrast-Enhanced Breast MRI for Robust Registration. , 2007, 10, 933-941.		20

#	Article	IF	CITATIONS
487	Low-Rank Total Variation for Image Super-Resolution. Lecture Notes in Computer Science, 2013, 16, 155-162.	1.0	20
488	Automatic Prostate MR Image Segmentation with Sparse Label Propagation and Domain-Specific Manifold Regularization. Lecture Notes in Computer Science, 2013, 23, 511-523.	1.0	19
489	Robust Anatomical Correspondence Detection by Hierarchical Sparse Graph Matching. IEEE Transactions on Medical Imaging, 2013, 32, 268-277.	5.4	19
490	Probabilistic MRI Brain Anatomical Atlases Based on 1,000 Chinese Subjects. PLoS ONE, 2013, 8, e50939.	1.1	19
491	Large deformation diffeomorphic registration of diffusion-weighted imaging data. Medical Image Analysis, 2014, 18, 1290-1298.	7.0	19
492	Estimating patientâ€specific and anatomically correct reference model for craniomaxillofacial deformity via sparse representation. Medical Physics, 2015, 42, 5809-5816.	1.6	19
493	Learning-Based Multimodal Image Registration for Prostate Cancer Radiation Therapy. Lecture Notes in Computer Science, 2016, 9902, 1-9.	1.0	19
494	Scalable joint segmentation and registration framework for infant brain images. Neurocomputing, 2017, 229, 54-62.	3.5	19
495	Low-Rank Representation for Multi-center Autism Spectrum Disorder Identification. Lecture Notes in Computer Science, 2018, 11070, 647-654.	1.0	19
496	Cognitive Assessment Prediction in Alzheimer's Disease by Multi-Layer Multi-Target Regression. Neuroinformatics, 2018, 16, 285-294.	1.5	19
497	Estimating Functional Connectivity Networks via Low-rank Tensor Approximation with Applications to MCI Identification. IEEE Transactions on Biomedical Engineering, 2019, 67, 1-1.	2.5	19
498	Dual-domain convolutional neural networks for improving structural information in 3â€⊤ MRI. Magnetic Resonance Imaging, 2019, 64, 90-100.	1.0	19
499	Longitudinal Prediction of Infant Diffusion MRI Data via Graph Convolutional Adversarial Networks. IEEE Transactions on Medical Imaging, 2019, 38, 2717-2725.	5.4	19
500	Fusion of ULS Group Constrained High- and Low-Order Sparse Functional Connectivity Networks for MCI Classification. Neuroinformatics, 2020, 18, 1-24.	1.5	19
501	Optimal Sparse Linear Prediction for Block-missing Multi-modality Data Without Imputation. Journal of the American Statistical Association, 2020, 115, 1406-1419.	1.8	19
502	Iterative Label Denoising Network: Segmenting Male Pelvic Organs in CT From 3D Bounding Box Annotations. IEEE Transactions on Biomedical Engineering, 2020, 67, 2710-2720.	2.5	19
503	MetricUNet: Synergistic image- and voxel-level learning for precise prostate segmentation via online sampling. Medical Image Analysis, 2021, 71, 102039.	7.0	19
504	Multi-task Dynamic Transformer Network for Concurrent Bone Segmentation and Large-Scale Landmark Localization with Dental CBCT. Lecture Notes in Computer Science, 2020, 12264, 807-816.	1.0	19

#	Article	IF	CITATIONS
505	DS-GCNs: Connectome Classification using Dynamic Spectral Graph Convolution Networks with Assistant Task Training. Cerebral Cortex, 2021, 31, 1259-1269.	1.6	19
506	Assessing clinical progression from subjective cognitive decline to mild cognitive impairment with incomplete multi-modal neuroimages. Medical Image Analysis, 2022, 75, 102266.	7.0	19
507	TSGCNet: Discriminative Geometric Feature Learning with Two-Stream Graph Convolutional Network for 3D Dental Model Segmentation. , 2021, , .		19
508	Follow My Eye: Using Gaze to Supervise Computer-Aided Diagnosis. IEEE Transactions on Medical Imaging, 2022, 41, 1688-1698.	5.4	19
509	Non-rigid registration between histological and MR images of the prostate: A joint segmentation and registration framework. , 2009, , .		18
510	Brain atlas fusion from high-thickness diagnostic magnetic resonance images by learning-based super-resolution. Pattern Recognition, 2017, 63, 531-541.	5.1	18
511	Discovering cortical sulcal folding patterns in neonates using largeâ€scale dataset. Human Brain Mapping, 2018, 39, 3625-3635.	1.9	18
512	Topological correction of infant white matter surfaces using anatomically constrained convolutional neural network. NeuroImage, 2019, 198, 114-124.	2.1	18
513	Super-resolution reconstruction of neonatal brain magnetic resonance images via residual structured sparse representation. Medical Image Analysis, 2019, 55, 76-87.	7.0	18
514	Local Diffusion Homogeneity Provides Supplementary Information in T2DM-Related WM Microstructural Abnormality Detection. Frontiers in Neuroscience, 2019, 13, 63.	1.4	18
515	Hierarchical Rough-to-Fine Model for Infant Age Prediction Based on Cortical Features. IEEE Journal of Biomedical and Health Informatics, 2020, 24, 214-225.	3.9	18
516	Difficulty-aware hierarchical convolutional neural networks for deformable registration of brain MR images. Medical Image Analysis, 2021, 67, 101817.	7.0	18
517	A Longitudinal MRI Study of Amygdala and Hippocampal Subfields for Infants with Risk of Autism. Lecture Notes in Computer Science, 2019, 11849, 164-171.	1.0	18
518	Feature Learning and Fusion of Multimodality Neuroimaging and Genetic Data for Multi-status Dementia Diagnosis. Lecture Notes in Computer Science, 2017, 10541, 132-140.	1.0	18
519	Tree-Guided Sparse Coding for Brain Disease Classification. Lecture Notes in Computer Science, 2012, 15, 239-247.	1.0	18
520	Sparse Patch Based Prostate Segmentation in CT Images. Lecture Notes in Computer Science, 2012, 15, 385-392.	1.0	18
521	Affine invariant detection of perceptually parallel 3D planar curves. Pattern Recognition, 2000, 33, 1909-1918.	5.1	17
522	Robust detection of skewed symmetries by combining local and semi-local affine invariants. Pattern Recognition, 2001, 34, 1417-1428.	5.1	17

#	Article	IF	CITATIONS
523	Structure-adaptive B-snake for segmenting complex objects. , 0, , .		17
524	Multi-Task Linear Programming Discriminant Analysis for the Identification of Progressive MCI Individuals. PLoS ONE, 2014, 9, e96458.	1.1	17
525	Learningâ€based subjectâ€specific estimation of dynamic maps of cortical morphology at missing time points in longitudinal infant studies. Human Brain Mapping, 2016, 37, 4129-4147.	1.9	17
526	A learning-based CT prostate segmentation method via joint transductive feature selection and regression. Neurocomputing, 2016, 173, 317-331.	3.5	17
527	Learningâ€based deformable image registration for infant <scp>MR</scp> images in the first year of life. Medical Physics, 2017, 44, 158-170.	1.6	17
528	Maximum Mean Discrepancy Based Multiple Kernel Learning for Incomplete Multimodality Neuroimaging Data. Lecture Notes in Computer Science, 2017, 10435, 72-80.	1.0	17
529	Learning-based structurally-guided construction of resting-state functional correlation tensors. Magnetic Resonance Imaging, 2017, 43, 110-121.	1.0	17
530	Densely Deep Supervised Networks with Threshold Loss for Cancer Detection in Automated Breast Ultrasound. Lecture Notes in Computer Science, 2018, , 641-648.	1.0	17
531	Infant Brain Development Prediction With Latent Partial Multi-View Representation Learning. IEEE Transactions on Medical Imaging, 2019, 38, 909-918.	5.4	17
532	Anatomy-Regularized Representation Learning for Cross-Modality Medical Image Segmentation. IEEE Transactions on Medical Imaging, 2021, 40, 274-285.	5.4	17
533	S3Reg: Superfast Spherical Surface Registration Based on Deep Learning. IEEE Transactions on Medical Imaging, 2021, 40, 1964-1976.	5.4	17
534	Synthesis and Inpainting-Based MR-CT Registration for Image-Guided Thermal Ablation of Liver Tumors. Lecture Notes in Computer Science, 2019, , 512-520.	1.0	17
535	Deep Ensemble Sparse Regression Network for Alzheimer's Disease Diagnosis. Lecture Notes in Computer Science, 2016, , 113-121.	1.0	17
536	Estimation of Brain Network Atlases Using Diffusive-Shrinking Graphs: Application to Developing Brains. Lecture Notes in Computer Science, 2017, 10265, 385-397.	1.0	17
537	Automated Segmentation of CBCT Image Using Spiral CT Atlases and Convex Optimization. Lecture Notes in Computer Science, 2013, 16, 251-258.	1.0	17
538	Incremental Learning With Selective Memory (ILSM): Towards Fast Prostate Localization for Image Guided Radiotherapy. IEEE Transactions on Medical Imaging, 2014, 33, 518-534.	5.4	16
539	In vivo MRI based prostate cancer localization with random forests and auto-context model. Computerized Medical Imaging and Graphics, 2016, 52, 44-57.	3.5	16
540	Learningâ€based deformable registration for infant <scp>MRI</scp> by integrating random forest with auto ontext model. Medical Physics, 2017, 44, 6289-6303.	1.6	16

#	Article	IF	CITATIONS
541	Joint Reconstruction and Segmentation ofÂ7T-like MR Images from 3T MRI Based onÂCascaded Convolutional Neural Networks. Lecture Notes in Computer Science, 2017, 10433, 764-772.	1.0	16
542	Domain Generalization forÂMammography Detection viaÂMulti-style and Multi-view Contrastive Learning. Lecture Notes in Computer Science, 2021, , 98-108.	1.0	16
543	Automatic Fetal Brain Extraction Using Multi-stage U-Net with Deep Supervision. Lecture Notes in Computer Science, 2019, , 592-600.	1.0	16
544	Temporal-Adaptive Graph Convolutional Network for Automated Identification of Major Depressive Disorder Using Resting-State fMRI. Lecture Notes in Computer Science, 2020, , 1-10.	1.0	16
545	Learning Distance Transform for Boundary Detection and Deformable Segmentation in CT Prostate Images. Lecture Notes in Computer Science, 2014, 8679, 93-100.	1.0	16
546	Joint 6D k-q Space Compressed Sensing for Accelerated High Angular Resolution Diffusion MRI. Lecture Notes in Computer Science, 2015, 24, 782-793.	1.0	16
547	Learning-Based Topological Correction for Infant Cortical Surfaces. Lecture Notes in Computer Science, 2016, 9900, 219-227.	1.0	16
548	Correlation-Weighted Sparse Group Representation for Brain Network Construction in MCI Classification. Lecture Notes in Computer Science, 2016, 9900, 37-45.	1.0	16
549	Learning Best Features and Deformation Statistics for Hierarchical Registration of MR Brain Images. Lecture Notes in Computer Science, 2007, 20, 160-171.	1.0	16
550	Improving Estimation of Fiber Orientations in Diffusion MRI Using Inter-Subject Information Sharing. Scientific Reports, 2016, 6, 37847.	1.6	15
551	Disrupted functional connectome in antisocial personality disorder. Brain Imaging and Behavior, 2017, 11, 1071-1084.	1.1	15
552	Frnet: Flattened Residual Network for Infant MRI Skull Stripping. , 2019, 2019, 999-1002.		15
553	Estimating sparse functional brain networks with spatial constraints for MCI identification. PLoS ONE, 2020, 15, e0235039.	1.1	15
554	Medical Image Retrieval Using Multi-graph Learning for MCI Diagnostic Assistance. Lecture Notes in Computer Science, 2015, 9350, 86-93.	1.0	15
555	Ensemble Hierarchical High-Order Functional Connectivity Networks for MCI Classification. Lecture Notes in Computer Science, 2016, 9901, 18-25.	1.0	15
556	4D Infant Cortical Surface Atlas Construction Using Spherical Patch-Based Sparse Representation. Lecture Notes in Computer Science, 2017, 10433, 57-65.	1.0	15
557	Temporally-Constrained Group Sparse Learning for Longitudinal Data Analysis. Lecture Notes in Computer Science, 2012, 15, 264-271.	1.0	15
558	Deep Multi-modal Latent Representation Learning for Automated Dementia Diagnosis. Lecture Notes in Computer Science, 2019, , 629-638.	1.0	15

#	Article	IF	CITATIONS
559	Joint estimation of multiple clinical variables of neurological diseases from imaging patterns. , 2010, , .		14
560	Reconstruction of super-resolution lung 4D-CT using patch-based sparse representation. , 2012, , .		14
561	Fiber-driven resolution enhancement of diffusion-weighted images. NeuroImage, 2014, 84, 939-950.	2.1	14
562	Detail-preserving construction of neonatal brain atlases in space-frequency domain. Human Brain Mapping, 2016, 37, 2133-2150.	1.9	14
563	Can we predict subjectâ€specific dynamic cortical thickness maps during infancy from birth?. Human Brain Mapping, 2017, 38, 2865-2874.	1.9	14
564	A Generative Model for OCT Retinal Layer Segmentation by Groupwise Curve Alignment. IEEE Access, 2018, 6, 25130-25141.	2.6	14
565	Segmenting hippocampal subfields from 3T MRI with multi-modality images. Medical Image Analysis, 2018, 43, 10-22.	7.0	14
566	Single- and Multiple-Shell Uniform Sampling Schemes for Diffusion MRI Using Spherical Codes. IEEE Transactions on Medical Imaging, 2018, 37, 185-199.	5.4	14
567	Task Decomposition and Synchronization for Semantic Biomedical Image Segmentation. IEEE Transactions on Image Processing, 2020, 29, 7497-7510.	6.0	14
568	Real-Time Quality Assessment of Pediatric MRI via Semi-Supervised Deep Nonlocal Residual Neural Networks. IEEE Transactions on Image Processing, 2020, 29, 7697-7706.	6.0	14
569	CT Male Pelvic Organ Segmentation via Hybrid Loss Network With Incomplete Annotation. IEEE Transactions on Medical Imaging, 2020, 39, 2151-2162.	5.4	14
570	DIKA-Nets: Domain-invariant knowledge-guided attention networks for brain skull stripping of early developing macaques. NeuroImage, 2021, 227, 117649.	2.1	14
571	Classification of type 2 diabetes mellitus with or without cognitive impairment from healthy controls using highâ€order functional connectivity. Human Brain Mapping, 2021, 42, 4671-4684.	1.9	14
572	Asymmetric multi-task attention network for prostate bed segmentation in computed tomography images. Medical Image Analysis, 2021, 72, 102116.	7.0	14
573	Cross-Model Attention-Guided Tumor Segmentation for 3D Automated Breast Ultrasound (ABUS) Images. IEEE Journal of Biomedical and Health Informatics, 2022, 26, 301-311.	3.9	14
574	End-to-End Dementia Status Prediction from Brain MRI Using Multi-task Weakly-Supervised Attention Network. Lecture Notes in Computer Science, 2019, , 158-167.	1.0	14
575	Constructing 4D Infant Cortical Surface Atlases Based on Dynamic Developmental Trajectories of the Cortex. Lecture Notes in Computer Science, 2014, 17, 89-96.	1.0	14
576	Learning-Based Meta-Algorithm for MRI Brain Extraction. Lecture Notes in Computer Science, 2011, 14, 313-321.	1.0	14

#	Article	IF	CITATIONS
577	Image mosaicking using SURF features of line segments. PLoS ONE, 2017, 12, e0173627.	1.1	14
578	Radiomics-based machine learning analysis and characterization of breast lesions with multiparametric diffusion-weighted MR. Journal of Translational Medicine, 2021, 19, 443.	1.8	14
579	Constructing Multi-View High-Order Functional Connectivity Networks for Diagnosis of Autism Spectrum Disorder. IEEE Transactions on Biomedical Engineering, 2022, 69, 1237-1250.	2.5	14
580	Deep learning derived automated <scp>ASPECTS</scp> on non ontrast <scp>CT</scp> scans of acute ischemic stroke patients. Human Brain Mapping, 2022, 43, 3023-3036.	1.9	14
581	Constructing Multi-frequency High-Order Functional Connectivity Network for Diagnosis of Mild Cognitive Impairment. Lecture Notes in Computer Science, 2017, 10511, 9-16.	1.0	13
582	Unpaired Deep Cross-Modality Synthesis with Fast Training. Lecture Notes in Computer Science, 2018, 11045, 155-164.	1.0	13
583	Voxel Deconvolutional Networks for 3D Brain Image Labeling. , 2018, 2018, 1226-1234.		13
584	Lung volume reduction and infection localization revealed in Big data CT imaging of COVID-19. International Journal of Infectious Diseases, 2021, 102, 316-318.	1.5	13
585	Statistical Representation and Simulation of High-Dimensional Deformations: Application to Synthesizing Brain Deformations. Lecture Notes in Computer Science, 2005, 8, 500-508.	1.0	13
586	CoCa-GAN: Common-Feature-Learning-Based Context-Aware Generative Adversarial Network for Glioma Grading. Lecture Notes in Computer Science, 2019, , 155-163.	1.0	13
587	Automatic Localization of Landmarks in Craniomaxillofacial CBCT Images Using a Local Attention-Based Graph Convolution Network. Lecture Notes in Computer Science, 2020, 12264, 817-826.	1.0	13
588	Designing Single- and Multiple-Shell Sampling Schemes for Diffusion MRI Using Spherical Code. Lecture Notes in Computer Science, 2014, 17, 281-288.	1.0	13
589	Structured Sparse Low-Rank Regression Model for Brain-Wide and Genome-Wide Associations. Lecture Notes in Computer Science, 2016, 9900, 344-352.	1.0	13
590	Feature Selection Based on Iterative Canonical Correlation Analysis for Automatic Diagnosis of Parkinson's Disease. Lecture Notes in Computer Science, 2016, 9901, 1-8.	1.0	13
591	XQ-NLM: Denoising Diffusion MRI Data via x-q Space Non-local Patch Matching. Lecture Notes in Computer Science, 2016, 9902, 587-595.	1.0	13
592	Two-Stream Graph Convolutional Network for Intra-Oral Scanner Image Segmentation. IEEE Transactions on Medical Imaging, 2022, 41, 826-835.	5.4	13
593	Consistent sulcal parcellation of longitudinal cortical surfaces. NeuroImage, 2011, 57, 76-88.	2.1	12
594	Anatomy-Guided Dense Individualized and Common Connectivity-Based Cortical Landmarks (A-DICCCOL). IEEE Transactions on Biomedical Engineering, 2015, 62, 1108-1119.	2.5	12

#	Article	IF	CITATIONS
595	Deformable MR Prostate Segmentation via Deep Feature Learning and Sparse Patch Matching. , 2017, , 197-222.		12
596	Locality Adaptive Multi-modality GANs for High-Quality PET Image Synthesis. Lecture Notes in Computer Science, 2018, 11070, 329-337.	1.0	12
597	Discriminative self-representation sparse regression for neuroimaging-based alzheimer's disease diagnosis. Brain Imaging and Behavior, 2019, 13, 27-40.	1.1	12
598	Image registration using machine and deep learning. , 2020, , 319-342.		12
599	Probing Tissue Microarchitecture of the Baby Brain via Spherical Mean Spectrum Imaging. IEEE Transactions on Medical Imaging, 2020, 39, 1-1.	5.4	12
600	Development of Dynamic Functional Architecture during Early Infancy. Cerebral Cortex, 2020, 30, 5626-5638.	1.6	12
601	Mammographic mass segmentation using multichannel and multiscale fully convolutional networks. International Journal of Imaging Systems and Technology, 2020, 30, 1095-1107.	2.7	12
602	Boundary Coding Representation for Organ Segmentation in Prostate Cancer Radiotherapy. IEEE Transactions on Medical Imaging, 2021, 40, 310-320.	5.4	12
603	NHBS-Net: A Feature Fusion Attention Network for Ultrasound Neonatal Hip Bone Segmentation. IEEE Transactions on Medical Imaging, 2021, 40, 3446-3458.	5.4	12
604	Multi-task Learning for Neonatal Brain Segmentation Using 3D Dense-Unet with Dense Attention Guided by Geodesic Distance. Lecture Notes in Computer Science, 2019, 11795, 243-251.	1.0	12
605	Prediction of Infant MRI Appearance and Anatomical Structure Evolution Using Sparse Patch-Based Metamorphosis Learning Framework. Lecture Notes in Computer Science, 2015, 9467, 197-204.	1.0	12
606	Does Manual Delineation only Provide the Side Information in CT Prostate Segmentation?. Lecture Notes in Computer Science, 2017, 10435, 692-700.	1.0	12
607	Image Registration by Hierarchical Matching of Local Spatial Intensity Histograms. Lecture Notes in Computer Science, 2004, , 582-590.	1.0	12
608	Inter-modality Relationship Constrained Multi-Task Feature Selection for AD/MCI Classification. Lecture Notes in Computer Science, 2013, 16, 308-315.	1.0	12
609	A Deep Learning Framework for Noise Component Detection from Resting-State Functional MRI. Lecture Notes in Computer Science, 2019, , 754-762.	1.0	12
610	GAN-Guided Deformable Attention Network for Identifying Thyroid Nodules in Ultrasound Images. IEEE Journal of Biomedical and Health Informatics, 2022, 26, 1582-1590.	3.9	12
611	Groupwise Registration via Graph Shrinkage on the Image Manifold. , 2013, , .		11
612	Uncertainty Estimation in Diffusion MRI Using the Nonlocal Bootstrap. IEEE Transactions on Medical Imaging, 2014, 33, 1627-1640.	5.4	11

#	Article	IF	CITATIONS
613	A Hybrid of Deep Network and Hidden Markov Model for MCI Identification with Resting-State fMRI. Lecture Notes in Computer Science, 2015, 9349, 573-580.	1.0	11
614	Functional MRI registration with tissueâ€specific patchâ€based functional correlation tensors. Human Brain Mapping, 2018, 39, 2303-2316.	1.9	11
615	Exploring diagnosis and imaging biomarkers of Parkinson's disease via iterative canonical correlation analysis based feature selection. Computerized Medical Imaging and Graphics, 2018, 67, 21-29.	3.5	11
616	Dual-Domain Cascaded Regression for Synthesizing 7T from 3T MRI. Lecture Notes in Computer Science, 2018, 11070, 410-417.	1.0	11
617	Surface-constrained volumetric registration for the early developing brain. Medical Image Analysis, 2019, 58, 101540.	7.0	11
618	Deep Learning Deformation Initialization for Rapid Groupwise Registration of Inhomogeneous Image Populations. Frontiers in Neuroinformatics, 2019, 13, 34.	1.3	11
619	Relationship between neuronal network architecture and naming performance in temporal lobe epilepsy: A connectome based approach using machine learning. Brain and Language, 2019, 193, 45-57.	0.8	11
620	Deep Bayesian Hashing With Center Prior for Multi-Modal Neuroimage Retrieval. IEEE Transactions on Medical Imaging, 2021, 40, 503-513.	5.4	11
621	Multiscale neural modeling of resting-state fMRI reveals executive-limbic malfunction as a core mechanism in major depressive disorder. NeuroImage: Clinical, 2021, 31, 102758.	1.4	11
622	Dilated perivascular space is related to reduced free-water in surrounding white matter among healthy adults and elderlies but not in patients with severe cerebral small vessel disease. Journal of Cerebral Blood Flow and Metabolism, 2021, 41, 2561-2570.	2.4	11
623	Learning Best Features for Deformable Registration of MR Brains. Lecture Notes in Computer Science, 2005, 8, 179-187.	1.0	11
624	Hierarchical Reconstruction of 7T-like Images from 3T MRI Using Multi-level CCA and Group Sparsity. Lecture Notes in Computer Science, 2015, 9350, 659-666.	1.0	11
625	Machine Learning Techniques for AD/MCI Diagnosis and Prognosis. Intelligent Systems Reference Library, 2014, , 147-179.	1.0	11
626	Wavelet-based Semi-supervised Adversarial Learning for Synthesizing Realistic 7T from 3T MRI. Lecture Notes in Computer Science, 2019, 11767, 786-794.	1.0	11
627	Recurrent Tissue-Aware Network for Deformable Registration of Infant Brain MR Images. IEEE Transactions on Medical Imaging, 2022, 41, 1219-1229.	5.4	11
628	D2FE-GAN: Decoupled dual feature extraction based GAN for MRI image synthesis. Knowledge-Based Systems, 2022, 252, 109362.	4.0	11
629	Diagnosis of Brain Abnormality Using both Structural and Functional MR Images. , 2006, 2006, 1044-7.		10
630	SIMULTANEOUS ESTIMATION AND SEGMENTATION OF T1 MAP FOR BREAST PARENCHYMA MEASUREMENT. , 2007, , .		10

#	Article	IF	CITATIONS
631	Diffusion tensor image registration using hybrid connectivity and tensor features. Human Brain Mapping, 2014, 35, 3529-3546.	1.9	10
632	Hierarchical and symmetric infant image registration by robust longitudinalâ€exampleâ€guided correspondence detection. Medical Physics, 2015, 42, 4174-4189.	1.6	10
633	An efficient radius-incorporated MKL algorithm for Alzheimer׳s disease prediction. Pattern Recognition, 2015, 48, 2141-2150.	5.1	10
634	Semi-supervised Hierarchical Multimodal Feature and Sample Selection for Alzheimer's Disease Diagnosis. Lecture Notes in Computer Science, 2016, 9901, 79-87.	1.0	10
635	Stability-Weighted Matrix Completion of Incomplete Multi-modal Data for Disease Diagnosis. Lecture Notes in Computer Science, 2016, 9901, 88-96.	1.0	10
636	Robust Fusion of Diffusion MRI Data for Template Construction. Scientific Reports, 2017, 7, 12950.	1.6	10
637	Fine-Grained Segmentation Using Hierarchical Dilated Neural Networks. Lecture Notes in Computer Science, 2018, , 488-496.	1.0	10
638	Construction of spatiotemporal infant cortical surface atlas of rhesus macaque. , 2018, 2018, 704-707.		10
639	XQ-SR: Joint x-q space super-resolution with application to infant diffusion MRI. Medical Image Analysis, 2019, 57, 44-55.	7.0	10
640	Multifold Acceleration of Diffusion MRI via Deep Learning Reconstruction from Slice-Undersampled Data. Lecture Notes in Computer Science, 2019, 11492, 530-541.	1.0	10
641	Guest Editorial Skin Lesion Image Analysis for Melanoma Detection. IEEE Journal of Biomedical and Health Informatics, 2019, 23, 479-480.	3.9	10
642	Low-rank dimensionality reduction for multi-modality neurodegenerative disease identification. World Wide Web, 2019, 22, 907-925.	2.7	10
643	FCN Based Label Correction for Multi-Atlas Guided Organ Segmentation. Neuroinformatics, 2020, 18, 319-331.	1.5	10
644	Estimating Reference Shape Model for Personalized Surgical Reconstruction of Craniomaxillofacial Defects. IEEE Transactions on Biomedical Engineering, 2021, 68, 362-373.	2.5	10
645	iCOVID: interpretable deep learning framework for early recovery-time prediction of COVID-19 patients. Npj Digital Medicine, 2021, 4, 124.	5.7	10
646	Registering Histological and MR Images of Prostate for Image-Based Cancer Detection. Lecture Notes in Computer Science, 2006, 9, 620-628.	1.0	10
647	Tract Dictionary Learning for Fast and Robust Recognition of Fiber Bundles. Lecture Notes in Computer Science, 2020, 12267, 251-259.	1.0	10
648	Joint Diagnosis and Conversion Time Prediction ofÂProgressive Mild Cognitive Impairment (pMCI) Using Low-Rank Subspace Clustering and Matrix Completion. Lecture Notes in Computer Science, 2015, 9351, 527-534.	1.0	10

#	Article	IF	CITATIONS
649	Neighborhood Matching for Curved Domains with Application to Denoising in Diffusion MRI. Lecture Notes in Computer Science, 2017, 10433, 629-637.	1.0	10
650	Multi-label Inductive Matrix Completion for Joint MGMT and IDH1 Status Prediction for Glioma Patients. Lecture Notes in Computer Science, 2017, 10434, 450-458.	1.0	10
651	Spatial-Temporal Constraint for Segmentation of Serial Infant Brain MR Images. Lecture Notes in Computer Science, 2010, , 42-50.	1.0	10
652	Estimating the 4D Respiratory Lung Motion by Spatiotemporal Registration and Building Super-Resolution Image. Lecture Notes in Computer Science, 2011, 14, 532-539.	1.0	10
653	Graph-Constrained Sparse Construction of Longitudinal Diffusion-Weighted Infant Atlases. Lecture Notes in Computer Science, 2017, 10433, 49-56.	1.0	10
654	COVIDSum: A linguistically enriched SciBERT-based summarization model for COVID-19 scientific papers. Journal of Biomedical Informatics, 2022, 127, 103999.	2.5	10
655	Common feature learning for brain tumor MRI synthesis by context-aware generative adversarial network. Medical Image Analysis, 2022, 79, 102472.	7.0	10
656	HAMMER: hierarchical attribute matching mechanism for elastic registration. , 0, , .		9
657	Hierarchical alignment of breast DCE-MR images by groupwise registration and robust feature matching. Medical Physics, 2011, 39, 353-366.	1.6	9
658	Discriminative Brain Effective Connectivity Analysis for Alzheimer's Disease: A Kernel Learning Approach upon Sparse Gaussian Bayesian Network. , 2013, 2013, 2243-2250.		9
659	Multidirectional and Topography-based Dynamic-scale Varifold Representations with Application to Matching Developing Cortical Surfaces. NeuroImage, 2016, 135, 152-162.	2.1	9
660	Automatic cystocele severity grading in transperineal ultrasound by random forest regression. Pattern Recognition, 2017, 63, 551-560.	5.1	9
661	Multi-modal Neuroimaging Data Fusion via Latent Space Learning for Alzheimer's Disease Diagnosis. Lecture Notes in Computer Science, 2018, 11121, 76-84.	1.0	9
662	Malignant Brain Tumor Classification Using the Random Forest Method. Lecture Notes in Computer Science, 2018, , 14-21.	1.0	9
663	Inter-Network High-Order Functional Connectivity (IN-HOFC) and its Alteration in Patients with Mild Cognitive Impairment. Neuroinformatics, 2019, 17, 547-561.	1.5	9
664	Deep morphological simplification network (MS-Net) for guided registration of brain magnetic resonance images. Pattern Recognition, 2020, 100, 107171.	5.1	9
665	Folding drives cortical thickness variations. European Physical Journal: Special Topics, 2020, 229, 2757-2778.	1.2	9
666	Multi-Atlas Brain Parcellation Using Squeeze-and-Excitation Fully Convolutional Networks. IEEE Transactions on Image Processing, 2020, 29, 6864-6872.	6.0	9

#	Article	IF	CITATIONS
667	Hierarchical Nonlocal Residual Networks for Image Quality Assessment of Pediatric Diffusion MRI With Limited and Noisy Annotations. IEEE Transactions on Medical Imaging, 2020, 39, 3691-3702.	5.4	9
668	Estimating Brain Functional Networks Based on Adaptively-Weighted fMRI Signals for MCI Identification. Frontiers in Aging Neuroscience, 2020, 12, 595322.	1.7	9
669	Asymmetrical Multi-task Attention U-Net for the Segmentation of Prostate Bed in CT Image. Lecture Notes in Computer Science, 2020, 12264, 470-479.	1.0	9
670	Estimating Tissue Microstructure with Undersampled Diffusion Data via Graph Convolutional Neural Networks. Lecture Notes in Computer Science, 2020, 12267, 280-290.	1.0	9
671	Temporally Dynamic Resting-State Functional Connectivity Networks for Early MCI Identification. Lecture Notes in Computer Science, 2013, , 139-146.	1.0	9
672	Identification of Infants at Risk for Autism Using Multi-parameter Hierarchical White Matter Connectomes. Lecture Notes in Computer Science, 2015, 9352, 170-177.	1.0	9
673	Progressive Graph-Based Transductive Learning for Multi-modal Classification of Brain Disorder Disease. Lecture Notes in Computer Science, 2016, 9900, 291-299.	1.0	9
674	Hierarchical Attribute-Guided Symmetric Diffeomorphic Registration for MR Brain Images. Lecture Notes in Computer Science, 2012, 15, 90-97.	1.0	9
675	Prostate Segmentation by Sparse Representation Based Classification. Lecture Notes in Computer Science, 2012, 15, 451-458.	1.0	9
676	Neighborhood-Correction Algorithm for Classification of Normal and Malignant Cells. Lecture Notes in Bioengineering, 2019, , 73-82.	0.3	9
677	Multi-Class ASD Classification via Label Distribution Learning with Class-Shared and Class-Specific Decomposition. Medical Image Analysis, 2022, 75, 102294.	7.0	9
678	Automatic Grading Assessments for Knee MRI Cartilage Defects via Self-ensembling Semi-supervised Learning with Dual-Consistency. Medical Image Analysis, 2022, 80, 102508.	7.0	9
679	Segmenting CT prostate images using population and patient-specific statistics for radiotherapy. , 2009, June 28, 2009, 282-285.		8
680	Nonlocal atlasâ€guided multiâ€channel forest learning for human brain labeling. Medical Physics, 2016, 43, 1003-1019.	1.6	8
681	Spatioâ€angular consistent construction of neonatal diffusion MRI atlases. Human Brain Mapping, 2017, 38, 3175-3189.	1.9	8
682	Image denoising with morphology- and size-adaptive block-matching transform domain filtering. Eurasip Journal on Image and Video Processing, 2018, 2018, .	1.7	8
683	A Preliminary Volumetric MRI Study of Amygdala and Hippocampal Subfields in Autism During Infancy. , 2019, 2019, 1052-1056.		8
684	Hippocampal Segmentation From Longitudinal Infant Brain MR Images via Classification-Guided Boundary Regression. IEEE Access, 2019, 7, 33728-33740.	2.6	8

#	Article	IF	CITATIONS
685	Population-guided large margin classifier for high-dimension low-sample-size problems. Pattern Recognition, 2020, 97, 107030.	5.1	8
686	An Effective MR-Guided CT Network Training for Segmenting Prostate in CT Images. IEEE Journal of Biomedical and Health Informatics, 2020, 24, 2278-2291.	3.9	8
687	High-Order Laplacian Regularized Low-Rank Representation for Multimodal Dementia Diagnosis. Frontiers in Neuroscience, 2021, 15, 634124.	1.4	8
688	Brain Function Network: Higher Order vs. More Discrimination. Frontiers in Neuroscience, 2021, 15, 696639.	1.4	8
689	Deformable Registration of Brain Tumor Images Via a Statistical Model of Tumor-Induced Deformation. Lecture Notes in Computer Science, 2005, 8, 263-270.	1.0	8
690	Pair-Wise and Group-Wise Deformation Consistency in Deep Registration Network. Lecture Notes in Computer Science, 2020, , 171-180.	1.0	8
691	Joint Image Quality Assessment and Brain Extraction of Fetal MRI Using Deep Learning. Lecture Notes in Computer Science, 2020, , 415-424.	1.0	8
692	Brain Image Labeling Using Multi-atlas Guided 3D Fully Convolutional Networks. Lecture Notes in Computer Science, 2017, 10530, 12-19.	1.0	8
693	Groupwise Registration with Sharp Mean. Lecture Notes in Computer Science, 2010, 13, 570-577.	1.0	8
694	Unsupervised Conditional Consensus Adversarial Network for Brain Disease Identification with Structural MRI. Lecture Notes in Computer Science, 2019, , 391-399.	1.0	8
695	Breast Tumor Segmentation in DCE-MRI With Tumor Sensitive Synthesis. IEEE Transactions on Neural Networks and Learning Systems, 2023, 34, 4990-5001.	7.2	8
696	STEP: SPATIAL-TEMPORAL ENHANCEMENT PATTERN, FOR MR-BASED BREAST TUMOR DIAGNOSIS. , 2007, , .		7
697	A Learning Based Hierarchical Framework for Automatic Prostate Localization in CT Images. Lecture Notes in Computer Science, 2011, 6963, 1-9.	1.0	7
698	Identification of breast vascular calcium deposition in digital mammography by linear structure analysis. , 2012, , .		7
699	Resolution enhancement of lung 4D T via groupâ€sparsity. Medical Physics, 2013, 40, 121717.	1.6	7
700	Maximum-Margin Based Representation Learning from Multiple Atlases for Alzheimer's Disease Classification. Lecture Notes in Computer Science, 2014, 17, 212-219.	1.0	7
701	Predicting Alzheimer's Disease Cognitive Assessment via Robust Low-Rank Structured Sparse Model. , 2017, 2017, 3880-3886.		7
702	Joint representation of consistent structural and functional profiles for identification of common cortical landmarks. Brain Imaging and Behavior, 2018, 12, 728-742.	1.1	7

#	ARTICLE	IF	CITATIONS
703	Construction of spatiotemporal neonatal cortical surface atlases using a large-scale dataset. , 2018, 2018, 1056-1059.		7
704	Machine Learning in Medical Imaging. IEEE Journal of Biomedical and Health Informatics, 2019, 23, 1361-1362.	3.9	7
705	Asymmetry Spectrum Imaging for Baby Diffusion Tractography. Lecture Notes in Computer Science, 2019, 11492, 319-331.	1.0	7
706	Flexible Locally Weighted Penalized Regression With Applications on Prediction of Alzheimer's Disease Neuroimaging Initiative's Clinical Scores. IEEE Transactions on Medical Imaging, 2019, 38, 1398-1408.	5.4	7
707	A novel approach to multiple anatomical shape analysis: Application to fetal ventriculomegaly. Medical Image Analysis, 2020, 64, 101750.	7.0	7
708	Dynamic neural circuit disruptions associated with antisocial behaviors. Human Brain Mapping, 2021, 42, 329-344.	1.9	7
709	Gaussianization of Diffusion MRI Data Using Spatially Adaptive Filtering. Medical Image Analysis, 2021, 68, 101828.	7.0	7
710	Multi-Regression based supervised sample selection for predicting baby connectome evolution trajectory from neonatal timepoint. Medical Image Analysis, 2021, 68, 101853.	7.0	7
711	Reconstructing High-Quality Diffusion MRI Data from Orthogonal Slice-Undersampled Data Using Graph Convolutional Neural Networks. Lecture Notes in Computer Science, 2019, 11766, 529-537.	1.0	7
712	Joint Neuroimage Synthesis and Representation Learning for Conversion Prediction of Subjective Cognitive Decline. Lecture Notes in Computer Science, 2020, , 583-592.	1.0	7
713	Prediction of Longitudinal Development of Infant Cortical Surface Shape Using a 4D Current-Based Learning Framework. Lecture Notes in Computer Science, 2015, 24, 576-587.	1.0	7
714	Large Deformation Diffeomorphic Registration of Diffusion-Weighted Images with Explicit Orientation Optimization. Lecture Notes in Computer Science, 2013, 16, 27-34.	1.0	7
715	Joint Learning of Image Regressor and Classifier for Deformable Segmentation of CT Pelvic Organs. Lecture Notes in Computer Science, 2015, , 114-122.	1.0	7
716	Discovering Cortical Folding Patterns in Neonatal Cortical Surfaces Using Large-Scale Dataset. Lecture Notes in Computer Science, 2016, 9900, 10-18.	1.0	7
717	Dynamic Routing Capsule Networks for Mild Cognitive Impairment Diagnosis. Lecture Notes in Computer Science, 2019, 2019, 620-628.	1.0	7
718	Pre-operative Overall Survival Time Prediction for Glioblastoma Patients Using Deep Learning on Both Imaging Phenotype and Genotype. Lecture Notes in Computer Science, 2019, 11764, 415-422.	1.0	7
719	Identifying patch-level MSI from histological images of Colorectal Cancer by a Knowledge Distillation Model. , 2020, , .		7
720	A cascaded nested network for 3T brain MR image segmentation guided by 7T labeling. Pattern Recognition, 2022, 124, 108420.	5.1	7

#	Article	IF	CITATIONS
721	Multiscale functional connectome abnormality predicts cognitive outcomes in subcortical ischemic vascular disease. Cerebral Cortex, 2022, 32, 4641-4656.	1.6	7
722	Robust detection of skewed symmetries. , 0, , .		6
723	Learning-based prostate localization for image guided radiation therapy. , 2011, , .		6
724	Automatic parcellation of cortical surfaces using random forests. , 2015, 2015, 810-813.		6
725	Learningâ€based 3T brain MRI segmentation with guidance from 7T MRI labeling. Medical Physics, 2016, 43, 6588-6597.	1.6	6
726	Inter-subject Similarity Guided Brain Network Modeling for MCI Diagnosis. Lecture Notes in Computer Science, 2017, 10541, 168-175.	1.0	6
727	Angular Upsampling in Infant Diffusion MRI Using Neighborhood Matching in x-q Space. Frontiers in Neuroinformatics, 2018, 12, 57.	1.3	6
728	Early-Life Nutrition and Cognitive Development: Imaging Approaches. Nestle Nutrition Institute Workshop Series, 2019, 90, 121-135.	1.5	6
729	Two-Phase Incremental Kernel PCA for Learning Massive or Online Datasets. Complexity, 2019, 2019, 1-17.	0.9	6
730	<scp>Highâ€Resolution</scp> Breast <scp>MRI</scp> Reconstruction Using a Deep Convolutional Generative Adversarial Network. Journal of Magnetic Resonance Imaging, 2020, 52, 1852-1858.	1.9	6
731	CorLab-Net: Anatomical Dependency-Aware Point-Cloud Learning for Automatic Labeling of Coronary Arteries. Lecture Notes in Computer Science, 2021, , 576-585.	1.0	6
732	Constructing high-order functional connectivity network based on central moment features for diagnosis of autism spectrum disorder. PeerJ, 2021, 9, e11692.	0.9	6
733	ABCnet: Adversarial bias correction network for infant brain MR images. Medical Image Analysis, 2021, 72, 102133.	7.0	6
734	Anatomical-Landmark-Based Deep Learning for Alzheimer's Disease Diagnosis with Structural Magnetic Resonance Imaging. Intelligent Systems Reference Library, 2020, , 127-147.	1.0	6
735	Tight Graph Framelets for Sparse Diffusion MRI q-Space Representation. Lecture Notes in Computer Science, 2016, 9902, 561-569.	1.0	6
736	Identification of MCI Using Optimal Sparse MAR Modeled Effective Connectivity Networks. Lecture Notes in Computer Science, 2013, 16, 319-327.	1.0	6
737	Probing Brain Micro-architecture by Orientation Distribution Invariant Identification of Diffusion Compartments. Lecture Notes in Computer Science, 2019, 11766, 547-555.	1.0	6
738	A novel theorem on symmetries of 2D images. , 0, , .		5

#	Article	IF	CITATIONS
739	CLASSIC: Consistent Longitudinal Alignment and Segmentation for Serial Image Computing. Lecture Notes in Computer Science, 2005, 19, 101-113.	1.0	5
740	Diagnosis of Brain Abnormality Using both Structural and Functional MR Images. , 2006, Suppl, 6585-8.		5
741	STATISTICALLY-CONSTRAINED DEFORMABLE REGISTRATION OF MR BRAIN IMAGES. , 2007, , .		5
742	ABSORB: Atlas building by Self-Organized Registration and Bundling. , 2010, , .		5
743	More insights into early brain development through statistical analyses of eigen-structural elements of diffusion tensor imaging using multivariate adaptive regression splines. Brain Structure and Function, 2014, 219, 551-569.	1.2	5
744	Craniomaxillofacial Deformity Correction via Sparse Representation in Coherent Space. Lecture Notes in Computer Science, 2015, , 69-76.	1.0	5
745	Automatic Segmentation of Hippocampus for Longitudinal Infant Brain MR Image Sequence by Spatial-Temporal Hypergraph Learning. Lecture Notes in Computer Science, 2016, 9993, 1-8.	1.0	5
746	Multiatlas-Based Segmentation Editing With Interaction-Guided Patch Selection and Label Fusion. IEEE Transactions on Biomedical Engineering, 2016, 63, 1208-1219.	2.5	5
747	Exploring Gyral Patterns of Infant Cortical Folding Based on Multi-view Curvature Information. Lecture Notes in Computer Science, 2017, 10433, 12-20.	1.0	5
748	Developing Novel Weighted Correlation Kernels for Convolutional Neural Networks to Extract Hierarchical Functional Connectivities from fMRI for Disease Diagnosis. Lecture Notes in Computer Science, 2018, 11046, 1-9.	1.0	5
749	A Multi-Tissue Global Estimation Framework for Asymmetric Fiber Orientation Distributions. Lecture Notes in Computer Science, 2018, 11072, 45-52.	1.0	5
750	Spherical U-Net For Infant Cortical Surface Parcellation. , 2019, 2019, 1882-1886.		5
751	Deep feature descriptor based hierarchical dense matching for X-ray angiographic images. Computer Methods and Programs in Biomedicine, 2019, 175, 233-242.	2.6	5
752	Neuroimage-Based Consciousness Evaluation of Patients with Secondary Doubtful Hydrocephalus Before and After Lumbar Drainage. Neuroscience Bulletin, 2020, 36, 985-996.	1.5	5
753	Learning Brain Functional Networks With Latent Temporal Dependency for MCI Identification. IEEE Transactions on Biomedical Engineering, 2022, 69, 590-601.	2.5	5
754	A Novel Unit-Based Personalized Fingerprint Feature Selection Strategy for Dynamic Functional Connectivity Networks. Frontiers in Neuroscience, 2021, 15, 651574.	1.4	5
755	Attention-Guided Deep Domain Adaptation for Brain Dementia Identification with Multi-site Neuroimaging Data. Lecture Notes in Computer Science, 2020, , 31-40.	1.0	5
756	Longitudinal Guided Super-Resolution Reconstruction of Neonatal Brain MR Images. Lecture Notes in Computer Science, 2015, 8682, 67-76.	1.0	5

#	Article	IF	CITATIONS
757	Inter-modality Dependence Induced Data Recovery for MCI Conversion Prediction. Lecture Notes in Computer Science, 2019, , 186-195.	1.0	5
758	Estimating Reference Bony Shape Model for Personalized Surgical Reconstruction of Posttraumatic Facial Defects. Lecture Notes in Computer Science, 2019, 11768, 327-335.	1.0	5
759	Multi-stage Image Quality Assessment of Diffusion MRI via Semi-supervised Nonlocal Residual Networks. Lecture Notes in Computer Science, 2019, 11766, 521-528.	1.0	5
760	Multi-Layer Multi-View Classification for Alzheimer's Disease Diagnosis. Proceedings of the AAAI Conference on Artificial Intelligence, 2018, 2018, 4406-4413.	3.6	5
761	Deep attentive spatio-temporal feature learning for automatic resting-state fMRI denoising. NeuroImage, 2022, 254, 119127.	2.1	5
762	Automated Segmentation of White Matter Lesions in 3D Brain MR Images, using Multivariate Pattern Classification. , 0, , .		4
763	Registration of Brain Images with Tumors: Towards the Construction of Statistical Atlases for Therapy Planning. , 0, , .		4
764	Diffusion Tensor Image Registration with Combined Tract and Tensor Features. Lecture Notes in Computer Science, 2011, 14, 200-208.	1.0	4
765	iTree: Fast and accurate image registration based on the combinative and incremental tree. , 2011, , .		4
766	Consciousness Level and Recovery Outcome Prediction Using High-Order Brain Functional Connectivity Network. Lecture Notes in Computer Science, 2017, 10511, 17-24.	1.0	4
767	Measuring Spectral Inconsistency of Multispectral Images for Detection and Segmentation of Retinal Degenerative Changes. Scientific Reports, 2017, 7, 11288.	1.6	4
768	Joint Robust Imputation and Classification for Early Dementia Detection Using Incomplete Multi-modality Data. Lecture Notes in Computer Science, 2018, 11121, 51-59.	1.0	4
769	Penalized Geodesic Tractography for Mitigating Gyral Bias. Lecture Notes in Computer Science, 2018, 11072, 12-19.	1.0	4
770	Pelvic Organ Segmentation Using Distinctive Curve Guided Fully Convolutional Networks. IEEE Transactions on Medical Imaging, 2018, , 1-1.	5.4	4
771	Graph-Based Deep Learning forÂPrediction of Longitudinal Infant Diffusion MRI Data. Mathematics and Visualization, 2019, 2019, 133-141.	0.4	4
772	Multi-channel framelet denoising of diffusion-weighted images. PLoS ONE, 2019, 14, e0211621.	1.1	4
773	A New Image Similarity Metric for Improving Deformation Consistency in Graph-Based Groupwise Image Registration. IEEE Transactions on Biomedical Engineering, 2019, 66, 2192-2199.	2.5	4
774	Learning-Based Computer-Aided Prescription Model for Parkinson's Disease: A Data-Driven Perspective. IEEE Journal of Biomedical and Health Informatics, 2021, 25, 3258-3269.	3.9	4

#	Article	IF	CITATIONS
775	Editorial: Predictive Intelligence in Biomedical and Health Informatics. IEEE Journal of Biomedical and Health Informatics, 2020, 24, 333-335.	3.9	4
776	Advanced deep learning methods for biomedical information analysis: An editorial. Neural Networks, 2021, 133, 101-102.	3.3	4
777	Collaborative Image Synthesis and Disease Diagnosis for Classification of Neurodegenerative Disorders with Incomplete Multi-modal Neuroimages. Lecture Notes in Computer Science, 2021, , 480-489.	1.0	4
778	Reducing magnetic resonance image spacing by learning without ground-truth. Pattern Recognition, 2021, 120, 108103.	5.1	4
779	Multimodal MRI Acceleration via Deep Cascading Networks with Peer-Layer-Wise Dense Connections. Lecture Notes in Computer Science, 2021, , 329-339.	1.0	4
780	Surface-Volume Consistent Construction of Longitudinal Atlases for the Early Developing Brain. Lecture Notes in Computer Science, 2019, 11765, 815-822.	1.0	4
781	Intrinsic Patch-Based Cortical Anatomical Parcellation Using Graph Convolutional Neural Network on Surface Manifold. Lecture Notes in Computer Science, 2019, 11766, 492-500.	1.0	4
782	Anatomy-Guided Convolutional Neural Network for Motion Correction in Fetal Brain MRI. Lecture Notes in Computer Science, 2020, 12436, 384-393.	1.0	4
783	Parcellation of Infant Surface Atlas Using Developmental Trajectories of Multidimensional Cortical Attributes. Lecture Notes in Computer Science, 2015, 9351, 543-550.	1.0	4
784	Automated Segmentation of CBCT Image with Prior-Guided Sequential Random Forest. Lecture Notes in Computer Science, 2016, , 72-82.	1.0	4
785	Atlas Construction via Dictionary Learning and Group Sparsity. Lecture Notes in Computer Science, 2012, 15, 247-255.	1.0	4
786	Incremental Learning with Selective Memory (ILSM): Towards Fast Prostate Localization for Image Guided Radiotherapy. Lecture Notes in Computer Science, 2013, 16, 378-386.	1.0	4
787	LINKS: Learning-Based Multi-source IntegratioN FrameworK for Segmentation of Infant Brain Images. Lecture Notes in Computer Science, 2014, , 22-33.	1.0	4
788	Tensorial Spherical Polar Fourier Diffusion MRI with Optimal Dictionary Learning. Lecture Notes in Computer Science, 2015, 9349, 174-182.	1.0	4
789	Tensor Generalized Estimating Equations for Longitudinal Imaging Analysis. Statistica Sinica, 2019, 29, 1977-2005.	0.2	4
790	Interpretable Feature Learning Using Multi-output Takagi-Sugeno-Kang Fuzzy System for Multi-center ASD Diagnosis. Lecture Notes in Computer Science, 2019, , 790-798.	1.0	4
791	LDGAN: Longitudinal-Diagnostic Generative Adversarial Network for Disease Progression Prediction with Missing Structural MRI. Lecture Notes in Computer Science, 2020, , 170-179.	1.0	4
792	Alterations of dynamic redundancy of functional brain subnetworks in Alzheimer's disease and major depression disorders. NeuroImage: Clinical, 2022, 33, 102917.	1.4	4

#	Article	IF	CITATIONS
793	Predicting Brain Amyloid-β PET Grades with Graph Convolutional Networks Based on Functional MRI and Multi-Level Functional Connectivity. Journal of Alzheimer's Disease, 2022, 86, 1679-1693.	1.2	4
794	Exploiting Sparse Self-Representation and Particle Swarm Optimization for CNN Compression. IEEE Transactions on Neural Networks and Learning Systems, 2023, 34, 10266-10278.	7.2	4
795	Reconstruction of Standard-Dose Pet From Low-Dose Pet Via Dual-Frequency Supervision and Global Aggregation Module. , 2022, , .		4
796	Detecting reflection axes by energy minimisation. , 0, , .		3
797	DSPs See Gains in Their Impact on New Medical Imaging Designs [Special Reports. IEEE Signal Processing Magazine, 2010, 27, 6-134.	4.6	3
798	Automated DNA fiber tracking and measurement. , 2011, , .		3
799	Multi-contrast diffusion tensor image registration with structural MRI. , 2012, , .		3
800	A Statistical Framework for Inter-Group Image Registration. Neuroinformatics, 2012, 10, 367-378.	1.5	3
801	Embarrassingly Parallel Acceleration of Global Tractography via Dynamic Domain Partitioning. Frontiers in Neuroinformatics, 2016, 10, 25.	1.3	3
802	Composite large margin classifiers with latent subclasses for heterogeneous biomedical data. Statistical Analysis and Data Mining, 2016, 9, 75-88.	1.4	3
803	Joint Sparse and Low-Rank Regularized Multi-Task Multi-Linear Regression for Prediction of Infant Brain Development with Incomplete Data. Lecture Notes in Computer Science, 2017, 10433, 40-48.	1.0	3
804	Landmark-Based Alzheimer's Disease Diagnosis Using Longitudinal Structural MR Images. Lecture Notes in Computer Science, 2017, 10081, 35-45.	1.0	3
805	Multimodal Hyper-connectivity Networks for MCI Classification. Lecture Notes in Computer Science, 2017, 10433, 433-441.	1.0	3
806	Temporal Correlation Structure Learning for MCI Conversion Prediction. Lecture Notes in Computer Science, 2018, 11072, 446-454.	1.0	3
807	Enhancement of Perivascular Spaces Using a Very Deep 3D Dense Network. Lecture Notes in Computer Science, 2018, , 18-25.	1.0	3
808	Topological Correction of Infant Cortical Surfaces Using Anatomically Constrained U-Net. Lecture Notes in Computer Science, 2018, , 125-133.	1.0	3
809	A computational method for longitudinal mapping of orientation-specific expansion of cortical surface in infants. Medical Image Analysis, 2018, 49, 46-59.	7.0	3
810	Cortical Foldingprints for Infant Identification. , 2019, 2019, 396-399.		3

#	Article	IF	CITATIONS
811	Group sparse reduced rank regression for neuroimaging genetic study. World Wide Web, 2019, 22, 673-688.	2.7	3
812	6-Month Infant Brain Mri Segmentation Guided by 24-Month Data Using Cycle-Consistent Adversarial Networks. , 2020, 2020, .		3
813	Genetic Influences on Longitudinal Trajectories of Cortical Thickness and Surface Area during the First 2 Years of Life. Cerebral Cortex, 2021, , .	1.6	3
814	Automatic Accurate Infant Cerebellar Tissue Segmentation with Densely Connected Convolutional Network. Lecture Notes in Computer Science, 2018, 11046, 233-240.	1.0	3
815	Progressive Infant Brain Connectivity Evolution Prediction from Neonatal MRI Using Bidirectionally Supervised Sample Selection. Lecture Notes in Computer Science, 2019, , 63-72.	1.0	3
816	Automatic Detection of Craniomaxillofacial Anatomical Landmarks on CBCT Images Using 3D Mask R-CNN. Lecture Notes in Computer Science, 2019, , 130-137.	1.0	3
817	Infant Cognitive Scores Prediction with Multi-stream Attention-Based Temporal Path Signature Features. Lecture Notes in Computer Science, 2020, 12267, 134-144.	1.0	3
818	A Deep Spatial Context Guided Framework for Infant Brain Subcortical Segmentation. Lecture Notes in Computer Science, 2020, 12267, 646-656.	1.0	3
819	Disentangled Intensive Triplet Autoencoder for Infant Functional Connectome Fingerprinting. Lecture Notes in Computer Science, 2020, 12267, 72-82.	1.0	3
820	Sparse Multimodal Manifold-Regularized Transfer Learning for MCI Conversion Prediction. Lecture Notes in Computer Science, 2013, , 251-259.	1.0	3
821	Sparsity-Learning-Based Longitudinal MR Image Registration for Early Brain Development. Lecture Notes in Computer Science, 2014, , 1-8.	1.0	3
822	Novel Single and Multiple Shell Uniform Sampling Schemes for Diffusion MRI Using Spherical Codes. Lecture Notes in Computer Science, 2015, 9349, 28-36.	1.0	3
823	Super-Resolution Reconstruction of Diffusion-Weighted Images Using 4D Low-Rank and Total Variation. Mathematics and Visualization, 2016, 2015, 15-25.	0.4	3
824	Construction of Neonatal Diffusion Atlases via Spatio-Angular Consistency. Lecture Notes in Computer Science, 2016, 9993, 9-16.	1.0	3
825	GACDN: generative adversarial feature completion and diagnosis network for COVID-19. BMC Medical Imaging, 2021, 21, 154.	1.4	3
826	Prediction of Standard-Dose PET Image by Low-Dose PET and MRI Images. Lecture Notes in Computer Science, 2014, , 280-288.	1.0	3
827	Deep Learning for Fast and Spatially-Constrained Tissue Quantification from Highly-Undersampled Data in Magnetic Resonance Fingerprinting (MRF). Lecture Notes in Computer Science, 2018, 11046, 398-405.	1.0	3
828	Deep Modeling of Growth Trajectories for Longitudinal Prediction of Missing Infant Cortical Surfaces. Lecture Notes in Computer Science, 2019, , 277-288.	1.0	3

#	Article	IF	CITATIONS
829	Acceleration of High-Resolution 3D MR Fingerprinting via a Graph Convolutional Network. Lecture Notes in Computer Science, 2020, , 158-166.	1.0	3
830	Deep Disentangled Hashing with Momentum Triplets for Neuroimage Search. Lecture Notes in Computer Science, 2020, 12261, 191-201.	1.0	3
831	Characterizing Intra-soma Diffusion with Spherical Mean Spectrum Imaging. Lecture Notes in Computer Science, 2020, 12267, 354-363.	1.0	3
832	Stability of Al-Enabled Diagnosis of Parkinson's Disease: A Study Targeting Substantia Nigra in Quantitative Susceptibility Mapping Imaging. Frontiers in Neuroscience, 2021, 15, 760975.	1.4	3
833	Altered Connectedness of the Brain Chronnectome During the Progression to Alzheimer's Disease. Neuroinformatics, 2022, 20, 391-403.	1.5	3
834	A hierarchical deformable model using statistical and geometric information. , 0, , .		2
835	Statistically-based reorientation of diffusion tensor field. , 0, , .		2
836	Morphological classification of medical images using nonlinear support vector machines. , 0, , .		2
837	Resolution enhancement of lung 4D T data using multiscale interphase iterative nonlocal means. Medical Physics, 2013, 40, 051916.	1.6	2
838	Online updating of contextâ€aware landmark detectors for prostate localization in daily treatment CT images. Medical Physics, 2015, 42, 2594-2606.	1.6	2
839	Multitemplate-based multiview learning for Alzheimer's disease diagnosis. , 2016, , 259-297.		2
840	Multiple-Atlas Segmentation in Medical Imaging. , 2016, , 231-257.		2
841	Learning Appearance and Shape Evolution for Infant Image Registration in the First Year of Life. Lecture Notes in Computer Science, 2016, , 36-44.	1.0	2
842	Longitudinal multi-scale mapping of infant cortical folding using spherical wavelets. , 2017, , .		2
843	Revealing Regional Associations of Cortical Folding Alterations with In Utero Ventricular Dilation Using Joint Spectral Embedding. Lecture Notes in Computer Science, 2018, 11072, 620-627.	1.0	2
844	Estimation of shape and growth brain network atlases for connectomic brain mapping in developing infants. , 2018, 2018, 985-989.		2
845	A computational method for longitudinal mapping of orientation-specific expansion of cortical surface area in infants. , 2018, 2018, 683-686.		2
846	Fetal cortical parcellation based on growth patterns. , 2018, 2018, 696-699.		2

#	Article	IF	CITATIONS
847	Infant brain development prediction with latent partial multi-view representation learning. , 2018, 2018, 1048-1051.		2
848	Construction of 4D Neonatal Cortical Surface Atlases Using Wasserstein Distance. , 2019, 2019, 995-998.		2
849	Longitudinal Harmonization for Improving Tractography in Baby Diffusion MRI. Mathematics and Visualization, 2019, 2019, 183-191.	0.4	2
850	Hierarchical Representation For Ct Prostate Segmentation. , 2019, , .		2
851	Fast Groupwise Registration Using Multi-Level and Multi-Resolution Graph Shrinkage. Scientific Reports, 2019, 9, 12703.	1.6	2
852	Tissue Segmentation Using Sparse Non-negative Matrix Factorization ofÂSpherical Mean Diffusion MRI Data. Mathematics and Visualization, 2019, 2019, 69-76.	0.4	2
853	Meta-Network Analysis of Structural Correlation Networks Provides Insights Into Brain Network Development. Frontiers in Human Neuroscience, 2019, 13, 93.	1.0	2
854	Identifying Thyroid Nodules inÂUltrasound Images Through Segmentation-Guided Discriminative Localization. Lecture Notes in Computer Science, 2021, , 135-144.	1.0	2
855	A Few-Shot Learning Graph Multi-trajectory Evolution Network forÂForecasting Multimodal Baby Connectivity Development from aÂBaseline Timepoint. Lecture Notes in Computer Science, 2021, , 11-24.	1.0	2
856	A consistent deep registration network with group data modeling. Computerized Medical Imaging and Graphics, 2021, 90, 101904.	3.5	2
857	Morphology-Guided Prostate MRI Segmentation with Multi-slice Association. Lecture Notes in Computer Science, 2021, , 507-516.	1.0	2
858	Multi-layer Temporal Network Analysis Reveals Increasing Temporal Reachability and Spreadability in the First Two Years of Life. Lecture Notes in Computer Science, 2019, , 665-672.	1.0	2
859	Generating Dual-Energy Subtraction Soft-Tissue Images from Chest Radiographs via Bone Edge-Guided GAN. Lecture Notes in Computer Science, 2020, , 678-687.	1.0	2
860	Unsupervised Learning for Spherical Surface Registration. Lecture Notes in Computer Science, 2020, 12436, 373-383.	1.0	2
861	Space-Frequency Detail-Preserving Construction of Neonatal Brain Atlases. Lecture Notes in Computer Science, 2015, 9350, 255-262.	1.0	2
862	Block-Based Statistics for Robust Non-parametric Morphometry. Lecture Notes in Computer Science, 2015, 9467, 62-70.	1.0	2
863	Joint Discriminative and Representative Feature Selection for Alzheimer's Disease Diagnosis. Lecture Notes in Computer Science, 2016, 10019, 77-85.	1.0	2
864	Automatic Hippocampal Subfield Segmentation from 3T Multi-modality Images. Lecture Notes in Computer Science, 2016, 10019, 229-236.	1.0	2

#	Article	IF	CITATIONS
865	Robust Construction of Diffusion MRI Atlases with Correction for Inter-Subject Fiber Dispersion. Mathematics and Visualization, 2017, 2016, 113-121.	0.4	2
866	Efficient Groupwise Registration for Brain MRI by Fast Initialization. Lecture Notes in Computer Science, 2017, 10541, 150-158.	1.0	2
867	Sparse Patch-Guided Deformation Estimation for Improved Image Registration. Lecture Notes in Computer Science, 2012, , 54-62.	1.0	2
868	Online Discriminative Multi-atlas Learning for Isointense Infant Brain Segmentation. Lecture Notes in Computer Science, 2014, , 297-305.	1.0	2
869	q-Space Upsampling Using x-q Space Regularization. Lecture Notes in Computer Science, 2017, 10433, 620-628.	1.0	2
870	Graph-Kernel-Based Multi-task Structured Feature Selection on Multi-level Functional Connectivity Networks for Brain Disease Classification. Lecture Notes in Computer Science, 2019, , 27-35.	1.0	2
871	Revealing Developmental Regionalization of Infant Cerebral Cortex Based on Multiple Cortical Properties. Lecture Notes in Computer Science, 2019, 11765, 841-849.	1.0	2
872	Identification of Abnormal Circuit Dynamics in Major Depressive Disorder via Multiscale Neural Modeling of Resting-State fMRI. Lecture Notes in Computer Science, 2019, 11766, 682-690.	1.0	2
873	Characterizing Non-Gaussian Diffusion in Heterogeneously Oriented Tissue Microenvironments. Lecture Notes in Computer Science, 2019, 11766, 556-563.	1.0	2
874	Deep Granular Feature-Label Distribution Learning for Neuroimaging-Based Infant Age Prediction. Lecture Notes in Computer Science, 2019, 11767, 149-157.	1.0	2
875	A Computational Framework for Dissociating Development-Related from Individually Variable Flexibility in Regional Modularity Assignment in Early Infancy. Lecture Notes in Computer Science, 2020, 12267, 13-21.	1.0	2
876	LONGITUDINAL MULTI-SCALE MAPPING OF INFANT CORTICAL FOLDING USING SPHERICAL WAVELETS. Proceedings, 2017, 2017, 93-96.	0.0	2
877	End-to-End Dementia Status Prediction from Brain MRI Using Multi-task Weakly-Supervised Attention Network. , 2019, 11767, 158-167.		2
878	Predicting Genomic Alterations of Phosphatidylinositol-3 Kinase Signaling in Hepatocellular Carcinoma: A Radiogenomics Study Based on Next-Generation Sequencing and Contrast-Enhanced CT. Annals of Surgical Oncology, 2022, , 1.	0.7	2
879	Influence of Gonadal Steroids on Cortical Surface Area in Infancy. Cerebral Cortex, 2021, , .	1.6	2
880	A deformable template model based on fuzzy alignment algorithm. , 0, , .		1
881	A B-snake model using statistical and geometric information-applications to medical images. , 0, , .		1

#	Article	IF	CITATIONS
883	4D image warping for measurement of longitudinal brain changes. , 0, , .		1
884	Consistent sulcal parcellation of longitudinal cortical surfaces. , 2011, , .		1
885	Measuring longitudinally dynamic cortex development in infants by reconstruction of consistent cortical surfaces. , 2013, , .		1
886	Patch-driven neonatal brain MRI segmentation with sparse representation and level sets. , 2013, , .		1
887	Automatic Craniomaxillofacial Landmark Digitization via Segmentation-Guided Partially-Joint Regression Forest Model. Lecture Notes in Computer Science, 2015, , 661-668.	1.0	1
888	Subject-Specific Estimation of Missing Cortical Thickness Maps in Developing Infant Brains. Lecture Notes in Computer Science, 2016, 9601, 83-92.	1.0	1
889	Cross-Manifold Guidance in Deformable Registration of Brain MR Images. Lecture Notes in Computer Science, 2016, , 415-424.	1.0	1
890	Learning Pairwise-Similarity Guided Sparse Functional Connectivity Network for MCI Classification. , 2017, 2017, 917-922.		1
891	Spatiotemporal Analysis of Developing Brain Networks. Frontiers in Neuroinformatics, 2018, 12, 48.	1.3	1
892	A Novel Image-Specific Transfer Approach for Prostate Segmentation in MR Images. , 2018, 2018, 806-810.		1
893	O10.3. EARLY BRAIN AND COGNITIVE DEVELOPMENT IN CHILDREN AT RISK FOR SCHIZOPHRENIA. Schizophrenia Bulletin, 2018, 44, S103-S104.	2.3	1
894	Hippocampus segmentation in MR images: Multiatlas methods and deep learning methods. , 2021, , 181-215.		1
895	Skull Segmentation from CBCT Images via Voxel-Based Rendering. Lecture Notes in Computer Science, 2021, 12966, 615-623.	1.0	1
896	VertNet: Accurate Vertebra Localization and Identification Network from CT Images. Lecture Notes in Computer Science, 2021, , 281-290.	1.0	1
897	Learning to Synthesize 7 T MRI from 3 T MRI with Few Data by Deformable Augmentation. Lecture Notes in Computer Science, 2021, , 70-79.	1.0	1
898	Brain Disease Classification and Progression Using Machine Learning Techniques. , 2014, , 3-32.		1
899	Automated Parcellation of the Cortex Using Structural Connectome Harmonics. Lecture Notes in Computer Science, 2019, 11766, 475-483.	1.0	1
900	Two-Stage Mapping-Segmentation Framework for Delineating COVID-19 Infections from Heterogeneous CT Images. Lecture Notes in Computer Science, 2020, , 3-13.	1.0	1

#	Article	IF	CITATIONS
901	Denoising Diffusion-Weighted Images Using Grouped Iterative Hard Thresholding of Multi-Channel Framelets. Mathematics and Visualization, 2017, 2016, 49-59.	0.4	1
902	LATEST: Local AdapTivE and Sequential Training for Tissue Segmentation of Isointense Infant Brain MR Images. Lecture Notes in Computer Science, 2017, 2017, 26-34.	1.0	1
903	Inherent Structure-Guided Multi-view Learning for Alzheimer's Disease and Mild Cognitive Impairment Classification. Lecture Notes in Computer Science, 2015, 9352, 296-303.	1.0	1
904	Soft-Split Random Forest for Anatomy Labeling. Lecture Notes in Computer Science, 2015, 9352, 17-25.	1.0	1
905	Fast Neuroimaging-Based Retrieval for Alzheimer's Disease Analysis. Lecture Notes in Computer Science, 2016, 10019, 313-321.	1.0	1
906	Early Brain Functional Segregation and Integration Predict Later Cognitive Performance. Lecture Notes in Computer Science, 2017, , 116-124.	1.0	1
907	Developmental Patterns Based Individualized Parcellation of Infant Cortical Surface. Lecture Notes in Computer Science, 2017, 10433, 66-74.	1.0	1
908	Do Baby Brain Cortices that Look Alike at Birth Grow Alike During the First Year of Postnatal Development?. Lecture Notes in Computer Science, 2018, , 566-574.	1.0	1
909	Early Development of Infant Brain Complex Network. Lecture Notes in Computer Science, 2019, , 832-840.	1.0	1
910	Adaptive Thresholding of Functional Connectivity Networks for fMRI-Based Brain Disease Analysis. Lecture Notes in Computer Science, 2019, , 18-26.	1.0	1
911	Deep Learning Models with Applications to Brain Image Analysis. , 2020, , 433-462.		1
912	Construction of Spatiotemporal Infant Cortical Surface Functional Templates. Lecture Notes in Computer Science, 2020, 12267, 238-248.	1.0	1
913	A New Metric for Characterizing Dynamic Redundancy of Dense Brain Chronnectome and Its Application to Early Detection of Alzheimer's Disease. Lecture Notes in Computer Science, 2020, , 3-12.	1.0	1
914	Linking Adolescent Brain MRI to Obesity via Deep Multi-cue Regression Network. Lecture Notes in Computer Science, 2020, , 111-119.	1.0	1
915	Cerebellum Tissue Segmentation with Ensemble Sparse Learning. Proceedings of the International Society for Magnetic Resonance in Medicine Scientific Meeting and Exhibition., 2017, 25, .	0.5	1
916	Non-rigid Brain MRI Registration Using Two-stage Deep Perceptive Networks. Proceedings of the International Society for Magnetic Resonance in Medicine Scientific Meeting and Exhibition., 2018, 2018, .	0.5	1
917	Segmentation with varying contrasts of pediatric MRI. Advances in Magnetic Resonance Technology and Applications, 2021, 2, 265-286.	0.0	1

918 Statistically optimized biopsy strategy for the diagnosis of prostate cancer. , 0, , .

0

#	Article	IF	CITATIONS
919	Statistically-Constrained High-Dimensional Warping Using Wavelet-Based Priors. , 0, , .		Ο
920	Improve Brain Registration Using Machine Learning Methods. , 0, , .		0
921	Application and validation of registration framework for real-time atlas guided biopsy. , 2008, , .		0
922	Regularization of diffusion tensor field using coupled robust anisotropic diffusion filters. , 2009, , .		0
923	TIMER: Tensor Image Morphing for Elastic Registration. , 2009, , .		0
924	Regularization of diffusion tensor field using coupled robust anisotropic diffusion filters. , 2009, , .		0
925	TIMER: Tensor Image Morphing for Elastic Registration. , 2009, , .		0
926	Tissue probability map constrained 4D clustering algorithm for increased accuracy and robustness in SerialMR brain image segmentation. International Journal of Medical Engineering and Informatics, 2011, 3, 286.	0.2	0
927	Prostate Deformation From Rectal Balloon and Dosimetric Effects in Prostate Brachytherapy. International Journal of Radiation Oncology Biology Physics, 2014, 90, S870-S871.	0.4	0
928	Image-Guided Radiotherapy with Machine Learning. , 2015, , 157-192.		0
929	Cortical Surface-Based Construction of Individual Structural Network with Application to Early Brain Development Study. Lecture Notes in Computer Science, 2015, 9351, 560-568.	1.0	0
930	Efficient Groupwise Registration of MR Brain Images via Hierarchical Graph Set Shrinkage. Lecture Notes in Computer Science, 2018, 11070, 819-826.	1.0	0
931	Longitudinal Sparse Regression for Neuroimage Based Consciousness Assessing and Tracking of Hydrocephalus Patients. , 2018, , .		0
932	Block-Extraction and Haar Transform Based Linear Singularity Representation for Image Enhancement. Mathematical Problems in Engineering, 2019, 2019, 1-14.	0.6	0
933	Charting Development-Based Joint Parcellation Maps Of Human and Macaque Brains During Infancy. , 2019, 2019, 422-425.		0
934	Erratum to "Deep Learning for Fast and Spatially Constrained Tissue Quantification From Highly Accelerated Data in Magnetic Resonance Fingerprinting―[Oct 19 2364-2374]. IEEE Transactions on Medical Imaging, 2020, 39, 543-543.	5.4	0
935	Sparse Dictionary Learning for 3D Craniomaxillofacial Skeleton Estimation Based on 2D Face Photographs. , 2021, , 41-53.		0
936	Deep learning and generative adversarial networks in oral andÂmaxillofacial surgery. , 2021, , 55-82.		0

#	Article	IF	CITATIONS
937	Spine-Rib Segmentation and Labeling via Hierarchical Matching and Rib-Guided Registration. Lecture Notes in Computer Science, 2021, , 537-545.	1.0	0
938	Machine (Deep) Learning for Orthodontic CAD/CAM Technologies. , 2021, , 117-129.		0
939	Patient-Specific Reference Model for Planning Orthognathic Surgery. , 2021, , 105-114.		Ο
940	Machine Learning for CBCT Segmentation of Craniomaxillofacial Bony Structures. , 2021, , 3-13.		0
941	SU-E-T-276: Learning Statistical Correlations of Deformation for Adaptive Radiation Therapy of Prostate Cancer. Medical Physics, 2011, 38, 3550-3550.	1.6	0
942	SU-E-J-44: Reconstruction of 4D-CT from Single Free-Breathing 3D-CT for Image Guided Lung Radiotherapy. Medical Physics, 2011, 38, 3451-3452.	1.6	0
943	Brain-Cloud: A Generalized and Flexible Registration Framework for Brain MR Images. Lecture Notes in Computer Science, 2013, , 153-161.	1.0	Ο
944	SU-E-T-397: Include Organ Deformation Into Dose Calculation of Prostate Brachytherapy. Medical Physics, 2014, 41, 316-316.	1.6	0
945	WE-AB-BRA-05: Fully Automatic Segmentation of Male Pelvic Organs On CT Without Manual Intervention. Medical Physics, 2015, 42, 3653-3653.	1.6	Ο
946	Relationship Induced Multi-atlas Learning for Alzheimer's Disease Diagnosis. Lecture Notes in Computer Science, 2016, , 24-33.	1.0	0
947	Robust and Discriminative Brain Genome Association Study. Lecture Notes in Computer Science, 2019, 11767, 456-464.	1.0	0
948	CNS: CycleGAN-Assisted Neonatal Segmentation Model for Cross-Datasets. Lecture Notes in Computer Science, 2019, , 172-179.	1.0	0
949	Morphological Simplification of Brain MR Images by Deep Learning for Facilitating Deformable Registration. Lecture Notes in Computer Science, 2019, , 203-211.	1.0	0
950	Globally Optimized Super-Resolution of Diffusion MRI Data via Fiber Continuity. Lecture Notes in Computer Science, 2020, 12267, 260-269.	1.0	0
951	Gyral Growth Patterns of Macaque Brains Revealed by Scattered Orthogonal Nonnegative Matrix Factorization. Lecture Notes in Computer Science, 2020, , 394-403.	1.0	0
952	Surface-based analysis of the developing cerebral cortex. Advances in Magnetic Resonance Technology and Applications, 2021, , 287-307.	0.0	0
953	Fast Correction of Eddy-Current and Susceptibility-Induced Distortions Using Rotation-Invariant Contrasts. Lecture Notes in Computer Science, 2020, 12262, 34-43.	1.0	0
954	Learning Subnetwork Biomarkers via Hypergraph for Classification of Autism Disease. Proceedings of the International Society for Magnetic Resonance in Medicine Scientific Meeting and Exhibition., 2017, 2017, 1719.	0.5	0

#	Article	IF	CITATIONS
955	Future Trends of PET/MR and Utility of AI in Multi-Modal Imaging. , 2022, , 79-86.		0
956	Special issue on machine learning and deep learning in magnetic resonance. NMR in Biomedicine, 2022, 35, e4713.	1.6	0
957	Diagnosis of Brain Abnormality Using both Structural and Functional MR Images. Annual International Conference of the IEEE Engineering in Medicine and Biology Society, 2006, , .	0.5	Ο
958	Parallel Sinogram and Image Framework With Co-Training Strategy for Metal Artifact Reduction in Tooth Ct Images. , 2022, , .		0